cartilage was retracted and the PCA muscle was exposed. The entire PCA muscle of the left or the right side was placed in clear view, and the muscle was resected near the midportion of the muscle belly (Fig. 2A). Subsequently, the previously exposed ipsilateral recurrent laryngeal nerve was electrically stimulated. Compound muscle action potentials were measured with electrodes inserted into the distal area of the resected PCA muscle. A gelatin sponge was placed at the resection site. This sponge had been soaked with physiologic saline or the aforementioned cells (autologous BSCs, allogeneic BSCs, autologous IMCs, or allogeneic IMCs). Drops of fibrin glue (Bolheal; Kaketsuken, Kumamoto, Japan) were used for fixation (Fig. 2B). The thyroid cartilage was returned to its original position, and the skin was sutured.

Evaluations

Evaluations involved compound muscle action potential (CMAP) measurements (using MEM-7202 Neuropac 2; Nihon Kohden Corporation, Tokyo, Japan) for electrophysiologic evaluation, vocal fold movements using a video endoscope, and histologic specimens.

In the transplantation procedure (described earlier), CMAPs were measured just before and immediately after resection of the PCA muscle (Fig. 2 and 3). The loss of muscle function was confirmed (Fig. 3). Six months after the treatment, we measured CMAPs in all cases and determined whether or not PCA muscle motor function had been recovered.

An electronic video-endoscope system (BF type1T 240, CV240, CLV-U40D, Olympus Co., Tokyo, Japan) was used to observe vocal fold movements, and the loss of movement was confirmed after resection of the PCA muscle on the surgical side. Subsequently, vocal fold movements were checked over time with a video endoscope as an indicator of restoration of function. Moreover, to quantitate the recovery of vocal fold movement, we measured the ratio of the opening angle of the bilateral vocal folds using a video endoscope under sedation 6 months after the treatment (Fig. 4). We used this ratio to define complete recovery (more than 90%), partial recovery (20% to 90%), and no recovery (less than 20%).

Histopathologic specimens of the PCA muscles were prepared. Comparisons were made between the specimens of the cell transplantation and those of the controls.

RESULTS

Functional Recovery

Images from the video endoscope in Figure 4 show recovery of the left vocal fold's movement 6 months after autotransplantation of BSCs. Figure 4A and 4B show the left vocal fold immobile, but 6 months later, movement of the left vocal fold had recovered (Fig. 4C and 4D).

Figure 5 shows CMAPs 6 months after the treatment. In this figure, we could confirm the recovery of the PCA muscle motor function by electrophysiologic evaluation.

Table I shows the presence or absence of motor function recovery of the vocal folds using a video endoscope (n = 13) and the recovery rate of vocal fold movement. Motor function recovery was achieved using autotransplantation of BSCs and IMCs, but minimal or no motor function recovery was achieved using allotransplantation of either type of cell. Motor function recovery was not observed in any dog in the control group. The CMAP data were in accordance with the results of Table I.

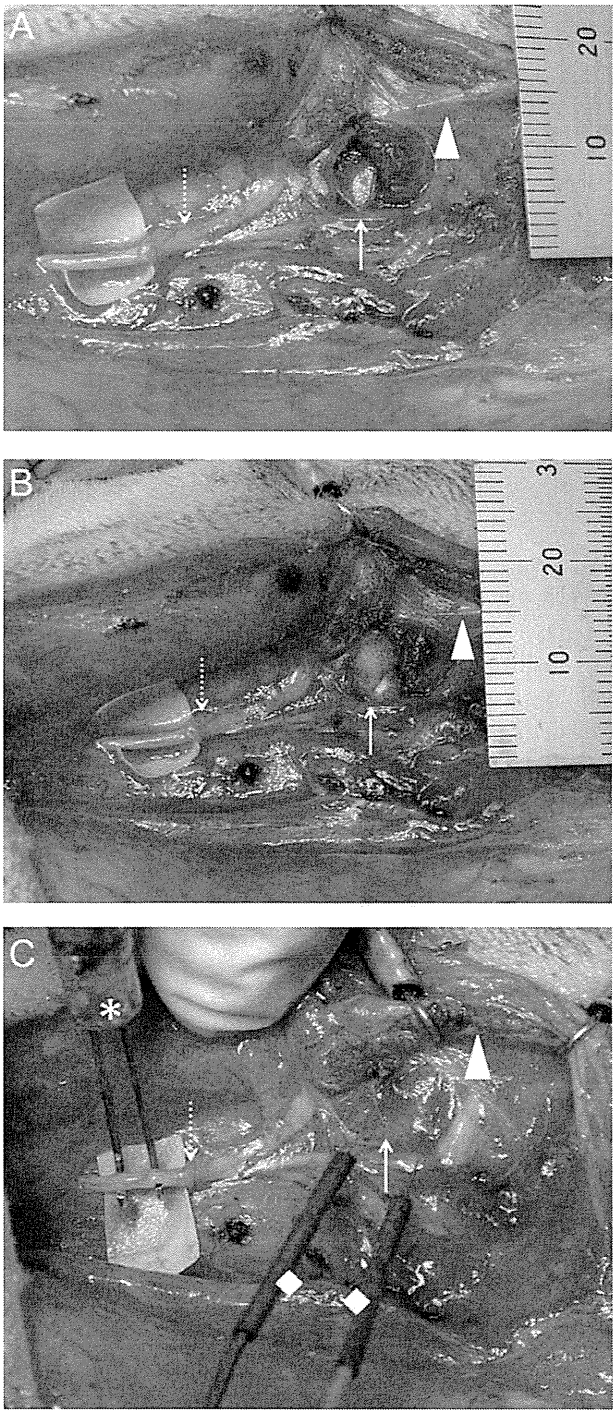

Fig. 2. (A) Exposure and resection of the posterior cricoarytenoid (PCA) muscle. Arrow: resected site of the PCA muscle; dashed arrow: recurrent laryngeal nerve; triangle: thyroid cartilage. (B) Transplantation of cells and scaffold. Arrow: transplanted cells and scaffold at the resected site of the PCA muscle; dashed arrow: recurrent laryngeal nerve; triangle: thyroid cartilage. (C) Measurement of compound muscle action potentials before resection of the PCA muscle. Arrow: resected site of the PCA muscle; dashed arrow: recurrent laryngeal nerve; triangle: thyroid cartilage; asterisk: nerve stimulator; diamond; needle electrode.

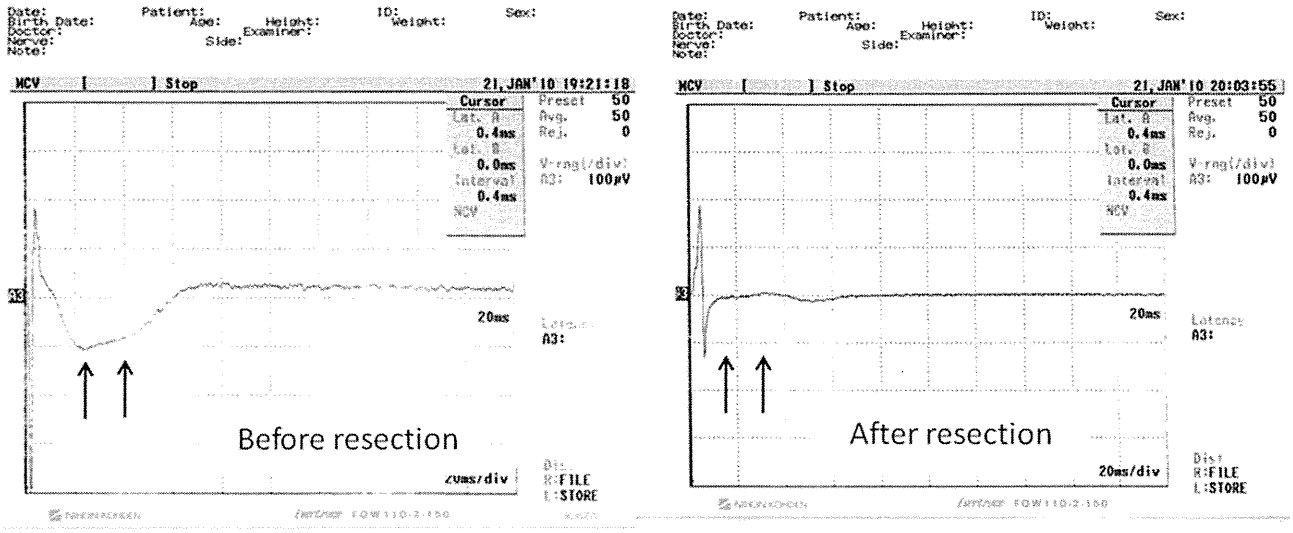

Fig. 3. Compound muscle action potentials (CMAPs) before and after resection; CMAP (arrow) was observed before resection but disappeared after resection.

The time required for functional recovery was compared for dogs with auto-BSC transplantation versus dogs with auto-IMC transplantation. The time required was approximately 2 months versus 3 to 4 months, respectively.

Histology

Figures 6 and 7 show the histopathologic specimens. In dogs with functional recovery, there was connective tissue in some areas of the transplanted site, and muscle regeneration was observed. In the control group, we observed the proliferation of irregular connective tissue to a much greater extent than observed with dogs undergoing functional recovery at the site of transplantation.

DISCUSSION

There have been many reports about the ability of MSCs to differentiate into muscles or mesodermal

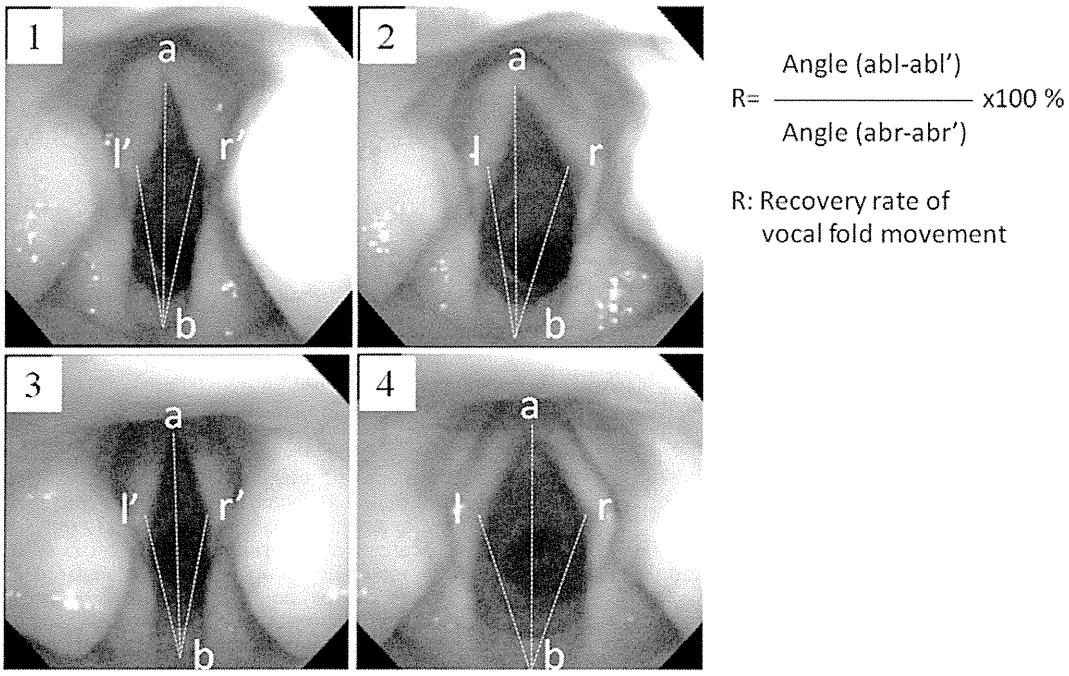

Fig. 4. Images from the video endoscope. (A, B) Immediately after resection of posterior cricoarytenoid muscle. (C, D) Six months after autotransplantation of bone marrow–derived stromal cells to the left side. We defined the recovery rate of vocal fold movement. A = anterior commissure; b = midportion of interarytenoid area; r, l (r', l') = junctional region of arytenoid cartilage and vocal ligament at opening position (r, l) and at resting respiratory position.

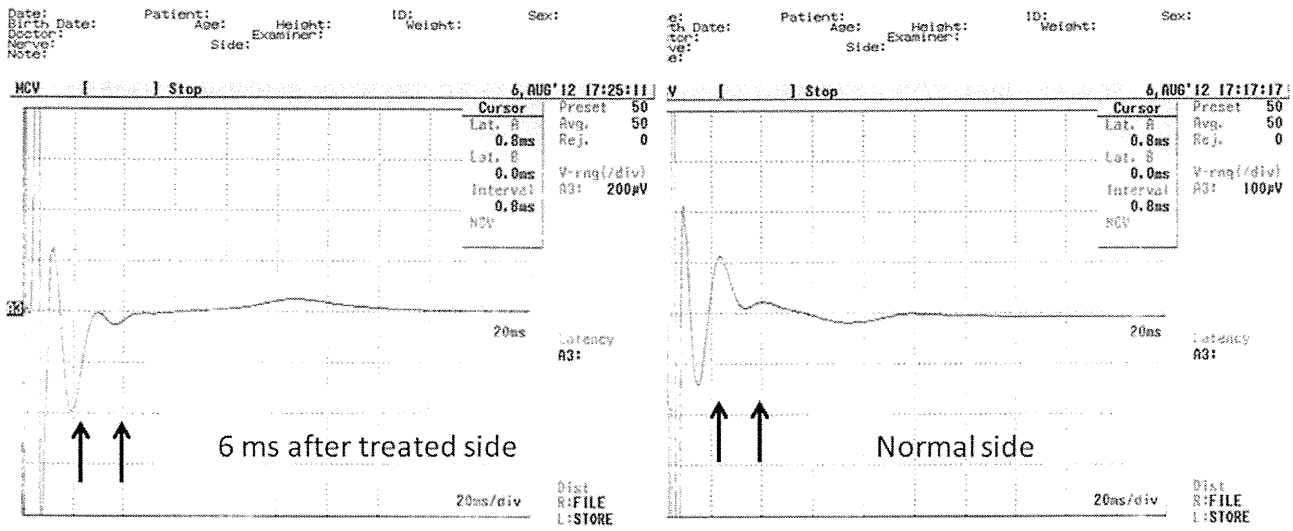

Fig. 5. Compound muscle action potentials (CMAPs) 6 months after autologous bone marrow–derived stromal cells, treated side and normal side in the same canine. CMAP (arrow) of the treated side recovered to the same extent as that of the normal side.

tissue.[4,5] However, Dezawa et al. were the first to develop a method for future clinical application which enabled MSCs to reliably differentiate into muscles.[1]

Some reports have shown that regenerated muscles regained their original functions, but these reports involved cardiac muscle functions of large animals or skeletal muscle motor functions of mice and rats.[6] Skeletal motor functions in mice and rats are more easily observed as recovery of lower limb movement. Restoration of skeletal motor function has not been shown in large animals. Large animals have not been used because for functional restoration of muscle cells, several things need to happen: 1) a large number of transplant cells need to be prepared, 2) regenerated muscle tissue needs to move consistently as one unit, and 3) motor function recovery needs to be observed clearly. These issues pose very difficult challenges. It has been known that telomeres shorten after each division of MSCs, and there are limitations to their division and proliferation.[7,8] Thus, it is very difficult to obtain cells in the range of 100 million. When BSCs are subcultured, the cell count does not increase beyond a certain number of generations. Many problems arise in efforts to demonstrate functional restoration of regenerated muscle. However, we found that the PCA muscle is an ideal target organ that meets all of the above conditions. Therefore, we selected vocal folds as a target organ to show functional recovery of regenerated muscle as described in the introduction.

When tissue regeneration is performed, an appropriate environment is normally necessary for the three components of regeneration: cells, scaffold, and regulatory factors. Based on the concept of in situ tissue engineering, we predicted that some type of growth factor would be secreted from the surroundings of the PCA muscle after the trigger of PCA muscle resection. Thus, in this study, we directly transplanted only the cells and scaffold to the injured PCA muscle without the addition of regulatory factors and examined whether regeneration occurred.

A gelatin sponge has a relatively sparse structure, providing scaffold and spaces for cells to freely grow. When a gelatin sponge is imbedded in the tissue or body cavity, it liquefies and is absorbed within approximately 1 month.[9] A gelatin sponge adheres strongly to the wound surface and has been found to have similar hemostatic effects as fibrin.[10] A gelatin sponge has been reported to be useful as a scaffold in regenerative treatment in patients with tympanic membrane perforation.[11]

When autologous and allogeneic cell transplants were compared in our study, we found that the group treated by autologous transplantation had functional recovery, whereas the group receiving allogeneic transplants had poor functional recovery. This result could have occurred because the transplanted cells were rejected by the recipients. However, there are many reports that MSCs possess immunomodulatory properties.[12,13] MSCs are immunosuppressive, interacting with T lymphocytes, antigen-presenting cells, B lymphocytes,

TABLE I.
Functional Recovery of the Posterior Cricoarytenoid Muscle (N = 13).

	Complete Recovery	Partial Recovery	No Recovery
Auto-BSCs	3		
Allo-BSCs			2
Auto-IMCs	1	2	
Allo-IMCs		1	1
Control			3

Allo = allogeneic; Auto = autologous; BSC = bone marrow–derived stromal cell; IMC = induced-muscle progenitor cell.

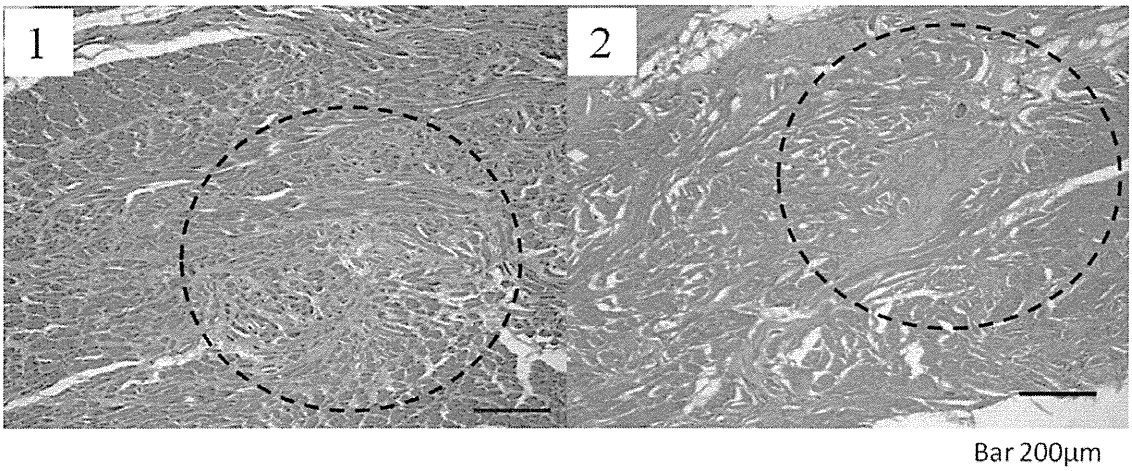

Fig. 6. Pathologic specimens 6 months after resection of posterior cricoarytenoid muscle and transplantation (hematoxylin and eosin stain). The black dotted line is the resected site of the muscle. (A) Dog with autologous bone marrow–derived stromal cell transplantation and functional recovery. (B) Control without functional recovery.

and natural killer cells. In addition, they are immunoprivileged, allowing transplantation across allogeneic barriers.[13] Our result contradicts the anticipated properties of MSCs. It is possible that other cells present in the MSC preparations may have caused rejection by the recipients. If muscle regeneration is to be applied to muscular degenerative diseases such as muscular dystrophy, allogeneic transplants will be necessary. Therefore, use of immunosuppressants might be required in the allogeneic transplantation group, an approach we will investigate in the next round of studies. Furthermore, there has been a report that MSCs promote malignant tumor formation.[14] Thus, this treatment methodology should not be applied for regeneration of muscle after resection of malignant tumors. However, clinical application of this method may still include a wide range of diseases and injuries.

Functional recovery was observed approximately 2 months after transplantation in the auto-BSC group and approximately 3 to 4 months after transplantation in the auto-IMC group, indicating faster recovery in the auto-BSC group. This finding suggested that the effects of transplanted cells in the process of muscle regeneration differed between these two groups. Based on our previous study,[3] we speculated that in auto-BSC transplantation, the transplanted cells remained as is without differentiation and that the following occurred simultaneously: the transplanted cells contributed to the improvement of the regenerative environment by paracrine and autocrine actions, and the transplanted cells directly differentiated into muscle tissue at the transplanted site. In the auto-IMC transplantation, it was thought that direct differentiation into muscle tissue occurred at the transplanted site without paracrine or autocrine action. More time

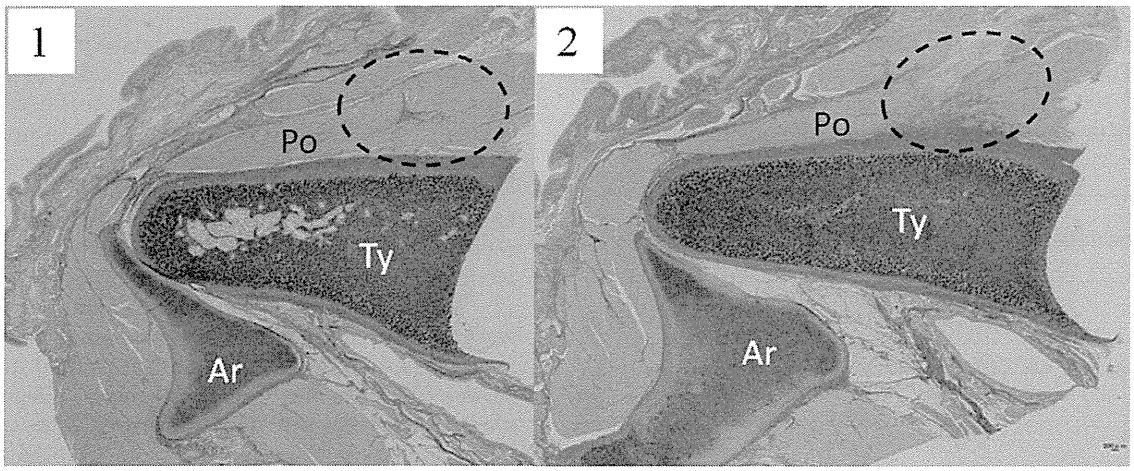

Fig. 7. Pathologic specimens 6 months after resection of the posterior cricoarytenoid muscle and transplantation (Elastica van Gieson stain). (A) Dog with autologous bone marrow–derived stromal cell transplantation and functional recovery. (B) Control without functional recovery. Dotted line indicates collagen fibers such as collagen stained pink. The dogs with good functional recovery had narrower scarred areas compared to those with poor functional recovery. Ar = arytenoid cartilage; Po = posterior cricoarytenoid muscle; Ty = thyroid cartilage.

might be required to achieve sufficient muscle regeneration and functional restoration using transplanted cells only. BSCs have a great potential for contributing paracrine and autocrine factors. However, this potential may be lost in proportion to BSCs' differentiation. Therefore, it is possible that IMCs have already lost this capacity.

Future topics of study include examination of the roles of transplanted cells.

CONCLUSION

Functional efficiency was shown in skeletal muscles regenerated using BSCs and induced muscle progenitor cells. Motor function recovery was observed using autologous transplantation of BSCs and induced muscle progenitor cells. Minimal functional recovery was observed using allogeneic transplantation of these cells. Muscle tissue regeneration in the transplanted site was observed in dogs with functional recovery after BSC transplantation. In the control group, instead of muscle regeneration, proliferation of irregular connective tissue was observed at the site of transplantation. The dogs with autologous transplantation of BSCs had faster functional recovery compared to dogs with autologous transplantation of induced muscle progenitor cells.

BIBLIOGRAPHY

1. Dezawa M, Ishikawa H, Itokazu Y, et al. Bone marrow stromal cells generate muscle cells and repair muscle degeneration. *Science* 2005;309:314–317.
2. Kanemaru S, Nakamura T, Kojima H, et al. Regeneration of the vocal cord using autologous mesenchymal stem cells. *Ann Otol Rhinol Laryngol* 2003;112:915–920.
3. Kanemaru S, Nakamura T, Yamashita M, et al. Destiny of the autologous bone marrow derived stromal cells implanted in the vocal fold. *Ann Otol Rhinol Laryngol* 2005;114:907–912.
4. Grove JE, Bruscia E, Krause DS. Plasticity of bone marrow-derived stem cells. *Stem Cell* 2004;22:487–500.
5. Beyer Nardi N, da Silva Meirelles L. Mesenchymal stem cells: isolation, in vitro expansion and characterization. *Handb Exp Pharmacol* 2006;249–282. http://www.ncbi.nlm.nih.gov/pubmed/16370331.
6. Winkler T, von Roth P, Matziolis G, et al. Dose-response relationship of mesenchymal stem cell transplantation and functional regeneration after severe skeletal muscle injury in rats. *Tissue Eng Part A* 2009;15:487–492.
7. Baxter MA, Wynn RF, Jowitt SN, et al. Study of telomere length reveals rapid aging of human marrow stromal cells following in vitro expansion. *Stem Cells* 2004;22:675–682.
8. Bonab MM, Alimoghaddam K, Talebian F, et al. Aging of mesenchymal stem cell in vitro. *BMC Cell Biol* 2006;10:7–14.
9. Correll JT, Prentice HR, Wise EC. Biological investigations of a new absorbable sponge. *Surg Gynecol Obstet* 1945;81:585–589.
10. Jenkins HP, Janda R, Clarke J. Clinical and experimental observations on the use of gelatin sponge or foam. *Surgery* 1946;20:124–132.
11. Kanemaru S, Umeda H, Kitani Y, et al. Regenerative treatment for tympanic membrane perforation. *Otol Neurotol* 2011;32:1218–1223.
12. Sordi V, Piemonti L. Therapeutic plasticity of stem cells and allograft tolerance. *Cytotherapy* 2011;13:647–660.
13. Larsen S, Lewis ID. Potential therapeutic applications of mesenchymal stromal cells. *Pathology* 2011;43:592–604.
14. Spaeth EL, Dembinski JL, Sasser AK, et al. Mesenchymal stem cell transition to tumor-associated fibroblasts contributes to fibrovascular network expansion and tumor progression. *PLoS One* 2009;4:e4992.

Cell Transplantation, Vol. 22, pp. 1613–1625, 2013
Printed in the USA.

0963-6897/13 $90.00 + .00
DOI: http://dx.doi.org/10.3727/096368912X658791
E-ISSN 1555-3892
www.cognizantcommunication.com

Transplantation of Bone Marrow Stromal Cell-Derived Neural Precursor Cells Ameliorates Deficits in a Rat Model of Complete Spinal Cord Transection

Misaki Aizawa-Kohama,*† Toshiki Endo,† Masaaki Kitada,* Shohei Wakao,*
Akira Sumiyoshi,‡ Dai Matsuse,* Yasumasa Kuroda,§ Takahiro Morita,*†
Jorge J. Riera,‡ Ryuta Kawashima,‡ Teiji Tominaga,† and Mari Dezawa*§

*Department of Stem Cell Biology and Histology, Tohoku University Graduate School of Medicine, Sendai, Japan
†Department of Neurosurgery, Tohoku University Graduate School of Medicine, Sendai, Japan
‡Institute of Development, Aging and Cancer, Tohoku University, Sendai, Japan
§Department of Anatomy and Anthropology, Tohoku University Graduate School of Medicine, Sendai, Japan

After severe spinal cord injury, spontaneous functional recovery is limited. Numerous studies have demonstrated cell transplantation as a reliable therapeutic approach. However, it remains unknown whether grafted neuronal cells could replace lost neurons and reconstruct neuronal networks in the injured spinal cord. To address this issue, we transplanted bone marrow stromal cell-derived neural progenitor cells (BM-NPCs) in a rat model of complete spinal cord transection 9 days after the injury. BM-NPCs were induced from bone marrow stromal cells (BMSCs) by gene transfer of the Notch-1 intracellular domain followed by culturing in the neurosphere method. As reported previously, BM-NPCs differentiated into neuronal cells in a highly selective manner in vitro. We assessed hind limb movements of the animals weekly for 7 weeks to monitor functional recovery after local injection of BM-NPCs to the transected site. To test the sensory recovery, we performed functional magnetic resonance imaging (fMRI) using electrical stimulation of the hind limbs. In the injured spinal cord, transplanted BM-NPCs were confirmed to express neuronal markers 7 weeks following the transplantation. Grafted cells successfully extended neurites beyond the transected portion of the spinal cord. Adjacent localization of synaptophysin and PSD-95 in the transplanted cells suggested synaptic formations. These results indicated survival and successful differentiation of BM-NPCs in the severely injured spinal cord. Importantly, rats that received BM-NPCs demonstrated significant motor recovery when compared to the vehicle injection group. Volumes of the fMRI signals in somatosensory cortex were larger in the BM-NPC-grafted animals. However, neuronal activity was diverse and not confined to the original hind limb territory in the somatosensory cortex. Therefore, reconstruction of neuronal networks was not clearly confirmed. Our results indicated BM-NPCs as an effective method to deliver neuronal lineage cells in a severely injured spinal cord. However, reestablishment of neuronal networks in completed transected spinal cord was still a challenging task.

Key words: Cell transplantation; Functional magnetic resonance imaging (fMRI); Bone marrow stromal cells (BMSCs); Neural progenitor cells (NPCs); Spinal cord injury (SCI)

INTRODUCTION

Spinal cord injury (SCI) induces local neural cell death and disruption of axonal pathways. Recovery is limited, since the central nervous system (CNS) environment deters axonal growth and regeneration through the actions of myelin inhibitors and astrocytes (14,45). Among the many experimental approaches to treat SCI, cell transplantation has the potential to repair or compensate for local spinal cord damage (5,15,27,32,44).

Bone marrow stromal cells (BMSCs) constitute a possible source of cells for autologous transplantation. They can be obtained from patient bone marrow aspirates and are readily expanded in vitro, which has made them a suitable candidate for clinical applications (9,11,34). We have established a method in which neural progenitor cells can be induced from BMSCs by introduction of the Notch-1 intracellular domain (NICD) followed by culturing using the neurosphere method (10,17). These progenitor cells, that is, bone marrow-derived neural progenitor cells (BM-NPCs), successfully formed spheres that highly expressed markers related to neural progenitors. When BM-NPCs were transplanted into a rat stroke model, they were shown to differentiate into neuronal cells, reconstruct synapses with host neurons, and lead to functional recovery of the animals (17).

Received October 7, 2011; final acceptance August 15, 2012. Online prepub date: October 31, 2012.
Address correspondence to Toshiki Endo, Department of Neurosurgery, Tohoku University Graduate School of Medicine, 1-1 Seiryo, Aoba, 980-8574, Sendai, Japan. Tel: +81-22-717-7230; Fax: +81-22-717-7233; E-mail: endo@nsg.med.tohoku.ac.jp *or* Mari Dezawa, Department of Stem Cell Biology and Histology and Department of Anatomy and Anthropology, Tohoku Univeristy Graduate School of Medicine, 2-1 Seiryo-machi, Aoba-ku, 980-8575, Sendai, Japan. Tel: +81-22-717-8025; Fax: +81-22-717-8030; E-mail: mdezawa@med.tohoku.ac.jp

In the present study, we newly applied BM-NPC transplantation to a rat model of complete spinal cord transection. The aim of this study is to confirm selective neuronal differentiation of the grafted BM-NPCs in the injured spinal cord and to achieve functional recovery. A possible means of achieving recovery from the injury would be the reconstruction of disrupted neuronal circuits between grafted cells and endogenous surrounding neurons, as suggested elsewhere (1). We employed immunohistochemistry to confirm neuronal differentiation of the grafted cells in the injured spinal cord. Synaptic formation of the BM-NPCs was evaluated with synaptophysin and postsynaptic density (PSD)-95. Retrograde tracing with fluorogold (FG) was utilized to see whether the BM-NPCs extended neurites across the transected portion of the spinal cord. We also used functional magnetic resonance imaging (fMRI) of the brain using blood oxygenation level-dependent (BOLD) contrast (12,13,30,40) to test sensory recovery and detect reestablishment of ascending neurotransmission across the injury. Behavioral analysis was included to evaluate locomotor recovery.

MATERIALS AND METHODS

Preparation of Marrow Stromal Cells and Neural Induction

All animal experiments were approved by the Animal Studies Ethics Committee of Tohoku University Graduate School of Medicine. Experimental procedures are presented in Figure 1. Numbers of animals used for each experiment were listed in Table 1. Rat BMSCs were isolated from adult female 10-week-old Wistar rats (CLEA Japan, Inc., Tokyo, Japan) according to methods described previously (4). Cells were maintained in α-minimum essential medium (α-MEM; Sigma, St. Louis, MO, USA) containing 10% fetal calf serum (FCS; Hyclone, Inc., Logan, UT, USA) and kanamycin (Wako Pure Chemical industries, Ltd., Osaka, Japan) at 37°C with 5% carbon dioxide. Next, the cells were transfected with a vector (pCI-neo-NICD) containing the mouse NICD (10). The NICD cDNA coded for a transmembrane region that included a small fragment of extracellular domain followed by a sequence encoding the entire intracellular domain of mouse Notch (initiating at amino acid 1,703 and terminating at the 3′-untranslated sequence).

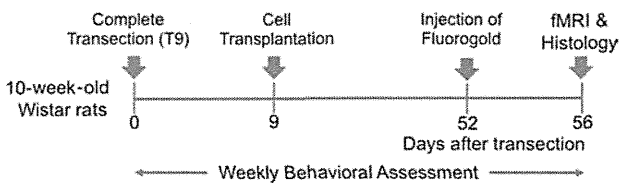

Figure 1. Experimental procedure. See Materials and Methods for detailed information. fMRI, functional magnetic resonance imaging.

Table 1. The Number of Animals per Experiments

	BBB Locomotor Scale	Fluorogold Tracing	fMRI Study	Total
Vehicle group	$n=14$	$n=4$	$n=6$	$n=14$
BM-NPCs group	$n=10$	$n=4$	$n=6$	$n=10$

BBB, Basso, Beattie, Bresnahan; BM-NPCs, bone marrow-derived neural progenitor cells; fMRI, functional magnetic resonance imaging.

This fragment was subcloned into a pCI-neo vector (Promega, Madison, WI, USA) and was transfected with BMSCs using Lipofectamine LTX (Invitrogen, Carlsbad, CA, USA) and selected using G418 (Invitrogen) for 5 days according to the manufacturer's instructions (10).

Induction of BM-NPCs

After G418 selection, rat NICD-transfected cells were washed and cultured in α-MEM containing 10% FCS for 2 days for recovery. The efficacy of NICD transfection was 98.8±0.8%, which is consistent with the previous report (10). During the expansion and recovery of transfected cells after G418 selection, green fluorescent protein (GFP) lentivirus (provided by Dr. D. Trono, Lausanne, Switzerland) was added to the culture medium for labelling purposes (29,39). Efficacy of GFP transfection was calculated three times. After recovery, the cells were washed and cultured in neurobasal medium supplied with B27 supplement (Invitrogen), 20 ng/ml of basic fibroblast growth factor and epidermal growth factor (both R&D Systems, Minneapolis, MN, USA) (17) at a cell density of 100,000 cells/ml on low cell-binding dishes (Nalgene Nunc, Rochester, NY, USA). After 8 days, generated spheres, namely BM-NPCs, were resuspended in Neurobasal medium to a concentration of approximately 30,000 cells/μl and transplanted to the injured rat spinal cord.

Immunocytochemistry

Spheres were fixed with 4% paraformaldehyde in 0.1 mol/L phosphate-buffered saline (PBS; both from Wako Pure Chemical Industries), collected by centrifugation, embedded in optimal cutting temperature (OCT) compound (Sakura Finetek Japan, Tokyo, Japan), and cut into 10-μm-thick sections using a cryostat (CM1850; Leica, Wetzlar, Germany). Samples were incubated with blocking solution containing 5% normal goat serum (Vector Laboratories, Burlingame, CA, USA), 0.1% Triton X-100 (Sigma), and 0.3% bovine serum albumin (BSA; Sigma) in 0.1 mol/L PBS at room temperature for 30 min. Samples were then incubated with primary antibodies in blocking solution overnight at 4°C. After three washes with 0.1 mol/L PBS, samples were incubated with secondary antibodies for 2 h at room temperature, followed by counterstaining with 4′,6-diamidino-2-phenylindole (DAPI) (for nuclear staining,

1:500; Sigma). The following primary antibodies were used for immunocytochemistry: anti-sex-determining region Y box 2 (Sox2; rabbit IgG, dilution 1:5,000; Chemicon, Temecula, CA, USA), anti-neurogenic differentiation (NeuroD; rabbit IgG, 1:200; Chemicon), anti-nestin (mouse IgG, 1:400; BD Pharmingen, San Jose, CA, USA), and anti-musashi (rabbit IgG, 1:200; Millipore, Billerica, MA, USA), anti-neuron-specific nuclear antigen (NeuN) (mouse IgG, 1:200; Chemicon), anti-glial fibrillary acidic protein (GFAP) (mouse IgG, 1:300; Sigma-Aldrich), and anti-oligodendrocyte marker 4 (O4; mouse IgM, 1:20; Millipore). These primary antibodies were detected with Alexa 488-conjugated anti-rabbit IgG or anti-mouse IgG antibodies (Molecular Probes, Invitrogen, Eugene, OR, USA) or Alexa 546-conjugated anti-rabbit IgG (1:500; Molecular Probes) or biotin-conjugated anti-mouse IgM (1:500; Jackson ImmunoResearch, West Grove, PA, USA) and streptavidin Alexa Fluor 488 (1:500; Molecular Probes) and streptavidin Alexa Fluor 680 (1:200; Molecular Probes). Percentages of immunopositive cells were calculated by comparing the cell numbers with the number of DAPI-positive cells. Cells in five fields, each including 100–500 cells, were counted in three independent cultures. Results were averaged and expressed as mean±SEM.

Complete Transection of the Midthoracic Spinal Cord (T9)

Adult, 10-week-old female Wistar rats weighing 200±20 g underwent complete transection of the spinal cord at the midthoracic level. Under isoflurane anesthesia (Wako Pure Chemical Industries), a laminectomy was performed at the T8–9 level. The spinal cord was exposed and transected completely using microscissors. Possible remaining adhesions were cut with a scalpel, and the rostral and caudal stumps were carefully lifted to verify complete transection. The dural incision was left open. Muscle and skin were sutured separately. The urinary bladder was emptied manually twice daily during the first week and once daily thereafter for 8 weeks.

Transplantation of BM-NPCs

Nine days after SCI rats were randomly assigned to groups receiving vehicle (vehicle group; $n=14$) or induced neural progenitor cells (BM-NPC group; $n=10$). Based on a previous report, the timing of transplantation was chosen to avoid delivering cells in an acute inflammatory stage following the injury or in chronic stage in which glial scar tissues would hinder regeneration of axons (31). The numbers of animals used in each experiment are shown in Table 1. Rats were reanesthetized and the thoracic spinal cord was carefully reexposed. Four injections were made with a depth of 1 mm, at 2 mm rostral and caudal of the lesion, and 0.5 mm left and right from the midline. At each site, 2.5 μl of cell suspension or vehicle (α-MEM; Sigma) was infused stereotactically using a Hamilton microsyringe attached to a glass micropipette at the rate of 0.5 μl/min (Hamilton, Reno, NV, USA). A total of 300,000 BM-NPCs were delivered to the spinal cord. The needles were left in the place for 1 min following each injection to prevent cells leaking from the site (2).

Immunohistochemical Analysis

Eight weeks after SCI, animals were anesthetized with an overdose of pentobarbiturate (Wako Pure Chemical Industries) and perfused transcardially with 4% paraformaldehyde in 0.1 mol/L PBS. Spinal cords were removed and embedded in OCT compound, and axial or sagittal slices were cut. Each spinal cord slice was cut into 10-μm sections using a cryostat. In three animals in each group, sagittal sections were used for neurofilament staining. The other immunohistochemical analyses were performed with axial slices. For immunostaining, the sections were washed with PBS and incubated with 5% normal goat serum, 0.3% Triton X-100, and 0.3% BSA in PBS (blocking solution) at room temperature for 30 min to block nonspecific binding. The slides were incubated with primary antibodies diluted in the blocking solution and incubated overnight at 4°C. After three washes with PBS containing 0.05% Triton X-100, the slides were incubated with secondary antibodies for 2 h at room temperature, followed by counterstaining with DAPI, which was diluted in PBS containing 0.1% Triton X-100. Sections were immunolabeled with the following primary antibodies: anti-neuron-specific class III β-tubulin (antibody name: Tuj-1; mouse IgG, 1:200; Sigma-Aldrich), anti-NeuN (mouse IgG, 1:200; Chemicon), anti-GFAP (mouse IgG, 1:300; Sigma-Aldrich), anti-O4 (mouse IgM, 1:20; Millipore), anti-synaptophysin (mouse IgG 1:1000; Chemicon), anti-PSD-95 (mouse IgG2a 1:100; Chemicon), anti-neurofilament (rabbit IgG, 1:200; Chemicon), and anti-GFP (chicken IgG, 1:1,000; Abcam, Philadelphia, PA, USA). Secondary antibodies were anti-mouse Alexa Fluor 568 (1:500; Molecular Probes), biotin-conjugated anti-chicken IgG (1:200; Jackson ImmunoResearch), anti-rabbit Alexa Fluor 568 (1:500; Molecular Probes), and streptavidin Alexa Fluor 488 (1:500; Molecular Probes). After immunolabeling, the samples were inspected under a confocal microscope system (C1si; Nikon, Tokyo, Japan). Using three animals in the BM-NPC group, transplanted cells in 20 fields in each cryosection were counted to confirm the survival of GFP-positive transplanted cells and evaluated the differentiation of BM-NPCs in the injured spinal cord. Results were averaged and expressed as mean±SEM.

Tracing Study

To label regenerated axons, FG (Fluorochrome, Denver, CO, USA) was injected into the spinal cord 4 days before the rats were killed (41). Using four rats in each group,

4% FG was injected into the spinal cord 10 mm caudal to the transected site over a period of 3 min using a microsyringe (24). After transcardiac perfusion, sections in the axial plane in the thoracic spinal cord including rostral and caudal ends of the transected site, cervical spinal cord, and the brain were stained with anti-FG (rabbit IgG, 1:200; Millipore) as a primary antibody and Alexa 568-conjugated anti-rabbit IgG (1:500, Molecular Probes) as a secondary antibody. Numbers of FG-positive grafted cells were counted at the rostral boundary of the transected spinal cord up to 5 mm from the transected stump. Results were averaged and expressed as mean ± SEM.

Locomotor Scale

Motor function in the hind limbs of all animals ($n=24$) was assessed using the Basso, Beattie, Bresnahan (BBB) locomotor rating scale on the day after injury and each week for 8 weeks after injury (6). Hind limb function was scored from 0 (flaccid paralysis) to 21 (normal gait) as a blind basis. The BM-NPC and vehicle groups were compared using multiple measurement analysis of variance (ANOVA) followed by Tukey's test. All values are given as mean ± SEM. For comparison, we also applied Mann–Whitney U test to evaluate BBB locomotor scale. A value of $p<0.05$ was considered statistically significant.

Functional MRI

Animal Preparation. Rats subjected to spinal cord transection and BM-NPC transplantation ($n=6$) or vehicle injection ($n=6$) underwent brain fMRI 8 weeks after injury, as described (25,40,42). Rats were first anesthetized with isoflurane (2.5% during induction and intubation) mixed with oxygen (30%) and air (70%). Rats were intubated and mechanically ventilated using a rodent ventilator (SAR-830AP Ventilator; CWE, Ardmore, PA, USA). A pair of small needle electrodes (NE-224S; Nihon-Koden, Tokyo Japan) was implanted subcutaneously in the left hind limb of each animal to deliver electrical stimulation. To confirm correct placement of the electrodes, a short sequence of current pulses (0.5 mA) was applied outside the magnet to evoke light muscle twitches. Next, a bolus of α-chloralose (20 mg/kg) (Sigma-Aldrich) was injected through the tail vein catheter, and 10 min later, the isoflurane was discontinued. Anesthesia was continued with α-chloralose infusion (20 mg/kg/h), and pancuronium bromide (2 mg/kg/h; Sigma-Aldrich Japan, Inc., Tokyo, Japan) was added for muscle relaxation. Rectal temperature was monitored and maintained at 37 ± 0.5°C using a water-circulating pad (CLEA Japan, Inc.) during the experiment.

fMRI Recordings. All MRI data were acquired using a 7T Bruker PharmaScan system (Bruker Biospin, Karlsruhe, Germany) with a 38-mm diameter birdcage coil. Prior to all MRI experiments, we first performed global magnetic field shimming inside the core and later completed shimming at the region of interest (ROI) by using a point-resolved spectroscopic protocol (37). Line width (full width at half maximum) at the end of the shimming procedure ranged from 15 to 20 Hz in the ROI (~300 μl). For the rat experiment, BOLD signals were obtained using gradient echo planar imaging (EPI) with the following parameters: repetition time (TR) = 1500 ms, echo time (TE) = 15 ms, spectral band width (SBW) = 250 kHz, field of view (FOV) = 25 × 14 mm^2, matrix size = 125 × 70, number of slices = 7, slice thickness = 1 mm, slice gap = 0 mm, number of volumes = 427, and number of dummy scans = 4.

Electrical Stimulation. A block design paradigm consisting of 10 blocks was employed, in which each block comprised 13 image packages of stimulation followed by 27 image packages of the resting condition. Electrical pulses were produced using a generator (SEN-3401; Nihon Koden) and an isolator (SS-203J, Nihon Koden). Pulsed currents of 10.0 mA with 0.3 ms duration and a constant frequency of 3 Hz were first delivered to the left hind limb of animals.

fMRI Data Analysis. Using statistical parametric mapping software (SPM2, Wellcome Department of Cognitive Neurology, London, UK), we normalized an individual rat's brain to the rat brain atlas template using the T2-weighted images (38). Spatial smoothing was performed using a Gaussian kernel of 0.6 mm full width at half maximum. Single-subject analysis was performed with a critical T value for each voxel calculated for the significance level of $p<0.001$. In response to the hind limb stimulation, volumes of significant clusters in cortex were compared between the groups using the Student's t test, after normal distribution of the data sets were confirmed using Kolmogorov–Smirnov test. We counted fMRI signals in bilateral somatosensory cortex. Activations were counted separately in the hind limb territory of the primary somatosensory cortex as well as the cortical areas medial and lateral to the hind limb area as defined in the rat atlas (36). Time course of BOLD signals (%) was depicted for the BM-NPC transplantation groups using a voxel [2.6, −2.0, −1.0] located in the original hind limb territory of primary somatosensory cortex (36). A single time course was created by averaging across all stimulation periods as described elsewhere (35). All values are given as mean ± SEM.

RESULTS

Grafted BM-NPCs Survived and Differentiated Into Neuronal Lineage Cells in the Injured Spinal Cord

In neurosphere culture, the NICD transfected BMSCs formed spheres. We examined the expression of nestin, NeuroD, Sox2, and musashi to determine whether these

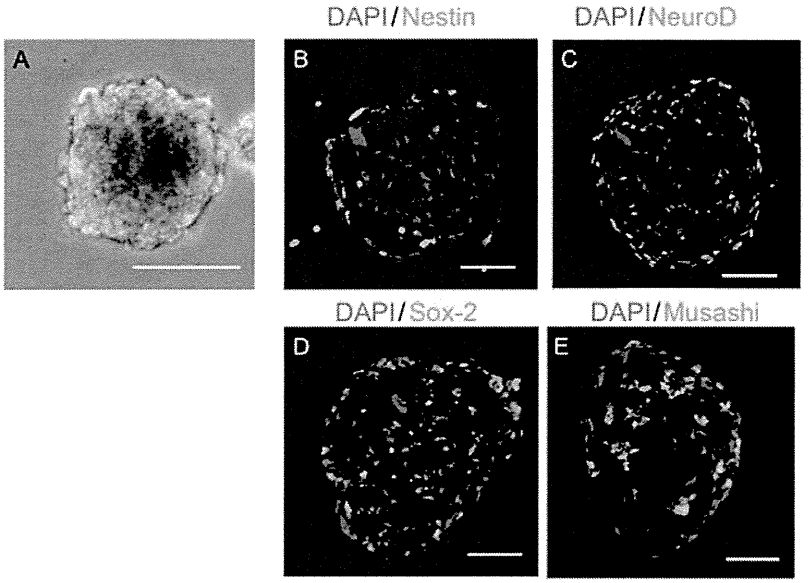

Figure 2. Induction of bone marrow-derived neural progenitor cells (BM-NPCs). (A) A phase contrast microscopy demonstrating BM-NPCs forming spheres on a low cell-binding dish. (B–E) Immunofluorescence images. Expression of nestin (B), neurogenic differentiation (NeuroD) (C), sex-determining region Y box 2 (Sox2) (D), and musashi (E) was confirmed. DAPI, 4′,6-diamidino-2-phenylindole. Scale bars: 50 μm.

spheres contained cells with neural progenitor cell markers. Spheres contained high percentages of cells positive for nestin (62.5±2.1%), NeuroD (82.3±2.1%), Sox2 (87.8±1.4%), and musashi (81.9±1.4%) (Fig. 2), while none of the cells were positive for NeuN (not shown). In addition, spheres did not contain cells positive for GFAP and O4 (not shown) suggesting that, consistent with the previous report, cells committed to the glial fate were not present in the sphere (17,28).

Next, BM-NPCs were transplanted into the injured spinal cord. Over 7 weeks after transplantation, no tumor formation was observed in any of the 10 spinal cords by inspection or histological analysis. Continuity of the spinal cord parenchyma was confirmed macroscopically and by neurofilament immunohistochemistry (Fig. 3A, B). Grafted cells were recognized in vivo by positive labeling of GFP. After transplantation of BM-NPCs 2 mm rostral and caudal to the transected portion of the spinal cord, grafted cells were confirmed to be located as far as 6 mm from the center of the injury (Fig. 3C–F). The total numbers of GFP-labeled cells were $8.02\pm0.71\times10^3$ in the injured spinal cord. Efficacy of GFP transfection was 45.0±4.4% in vitro. Accurate assessment of donor cell survival can only be pursued by counting all of the GFP signals in every spinal cord section. In this sense, there is a limitation of assessing the true measure of donor cell survival in our count, but the ratio of transplanted cells that survived in the injured spinal cord was estimated to be roughly 5.9%.

Importantly, BM-NPCs survived and showed low capacity for differentiating into astrocytes in the injured spinal cord. The frequencies of βIII tubulin (antibody Tuj-1)- and NeuN-positive cells among GFP-positive cells were 77.2±2.6% (Fig. 4A–E) and 36.0±3.2% (Fig. 4F–I), respectively. Nestin-positive cells were observed among the GFP-positive cells at the ratio of 9.7±2.0% (Fig. 4J–M), while the ratio of GFAP-positive cells was 2.9±0.9% (Fig. 4N–Q). O4 positive cells could not be detected (not shown). These observations suggested that the majority of the transplanted BM-NPCs became neuronal marker-positive cells. Moreover, the frequency of nestin-positive cells, which was 62.5±2.1% in vitro and 9.7±2.0% in vivo, indicated advancement of differentiation of the transplanted cells within the injured spinal cord, as nestin is potential indicator of neural differentiation (43). Spheres contained no cells positive for NeuN, while the frequency of NeuN-positive cells among GFP-positive cells increased in vivo, which also supported differentiation of the grafted cells. Transplanted cells were also found to express the synaptic marker synaptophysin (Fig. 5). Among GFP-positive cells, 24.2±2.2% were positive for synaptophysin. It was noted that synaptophysin was localized predominantly next to GFP-positive transplanted cells in a punctate pattern (Fig. 5). To further assess the synaptic formation between the transplanted cells and the host cells, immunohistochemistry for PSD-95 was performed (8,22). PSD-95 labeling was adjacent to the synaptophysin-positive signal in the transplanted cells (Fig. 6).

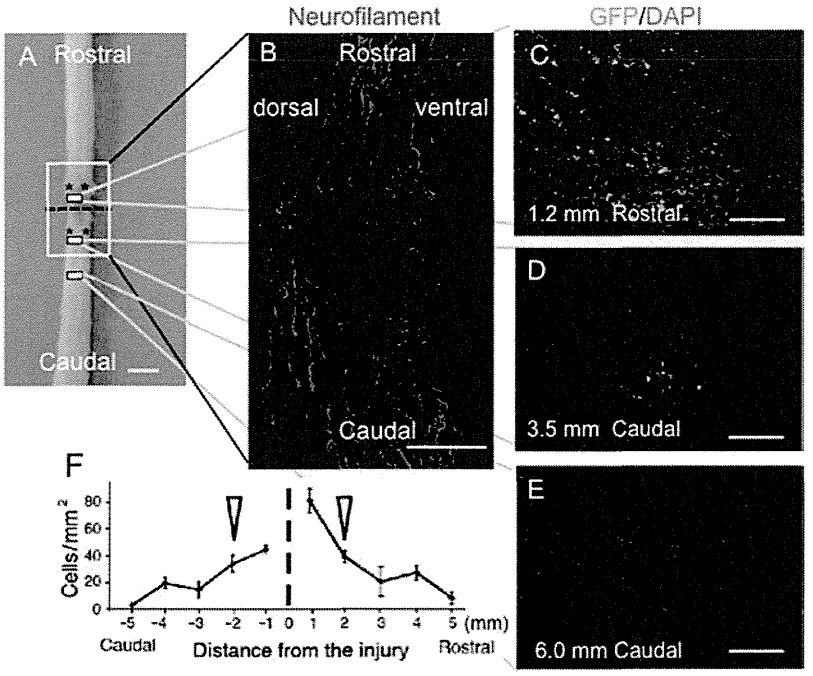

Figure 3. Transplanted bone marrow-derived neural progenitor cells (BM-NPCs) in the injured spinal cord 8 weeks after transection. (A) Schematic drawing of a representative spinal cord from the BM-NPC group showing sites of transection (dotted line) and transplantation (*). (B) Representative longitudinal section stained for neurofilaments corresponding to the white box in (A), showing anatomical continuity of spinal cord parenchyma at the injury site. (C–E) Distribution of green fluorescent protein (GFP)-positive transplanted cells at sites 1.2 mm rostral (C), 3.5 mm caudal (D), and 6.0 mm caudal (E) to the injury center in the dorsal spinal cord. Positions of the panels are indicated by small boxes in (A). (F) Numbers of GFP-positive cells between 5 mm caudal and 5 mm rostral to the injury center. The dotted line and arrowheads indicate the transected portion and the site of cell transplantation, respectively. Note that the GFP-positive cells were incorporated into the host spinal cord. DAPI, 4′,6-diamidino-2-phenylindole. Scale bars: 2 mm (A), 250 μm (B), 100 μm (C–E).

Fluorogold Tracing Detected Extension of Neurites From BM-NPCs Across the Transected Site in the Spinal Cord

Four days before the animals were sacrificed, we injected the retrograde tracer FG 10 mm caudal to the transected site, so that FG would be taken up through the terminals of the regenerated neurites (Fig. 7A). Strikingly, in the BM-NPC group, we detected FG-labeled grafted cells in the rostral as well as caudal spinal cord in all four rats (Fig. 7B–G). The presence of cells double positive for FG and GFP rostral to the transected portion indicated that the grafted cells extended their neurites across the transected portion to reach the caudal spinal cord. The site of injection was carefully examined to ensure that no FG could have reached the transected portion by diffusion (24). The number of cells labeled with FG and GFP at the rostral boundary of the transected spinal cord was $5.17 \pm 0.75/mm^2$ in the BM-NPC group. FG-labeled BM-NPCs were located rostrally 1.8 ± 0.18 mm from the transection stump to a maximum of 4.6 mm. In the vehicle group, no FG-labeled cells were found in the spinal cord rostral to the transected site. In any of the injured animals with or without treatments ($n=4$, each group), no FG-labeled cells were found in the cervical spinal cord or in the brain sections.

Behavioral Analysis Indicated Improved Hind Limb Locomotor Function After BM-NPC Transplantation

BBB locomotor scores for the BM-NPC and vehicle groups were determined each week for 8 weeks after injury (Fig. 8). Improvements in hind limb motor function were significantly greater in the BM-NPC group than in the vehicle group after 2 weeks ($p<0.01$) and over 3–8 weeks ($p<0.001$, repeated measures ANOVA followed by post hoc Tukey's test). Mann–Whitney U test also indicated significant functional recovery between 2 and 8 weeks (Fig. 8). Eight weeks after the injury, averaged BBB scale of injured animals was 3.31 in the control group while 5.80 in BM-NPCs transplantation group. Following the treatments, rats showed symptoms of recovery; they showed extensive movements of the three joints in the hind limbs. The difference between these groups was statistically significant ($p<0.001$, post hoc Tukey's test; $p<0.01$, Mann–Whitney U test).

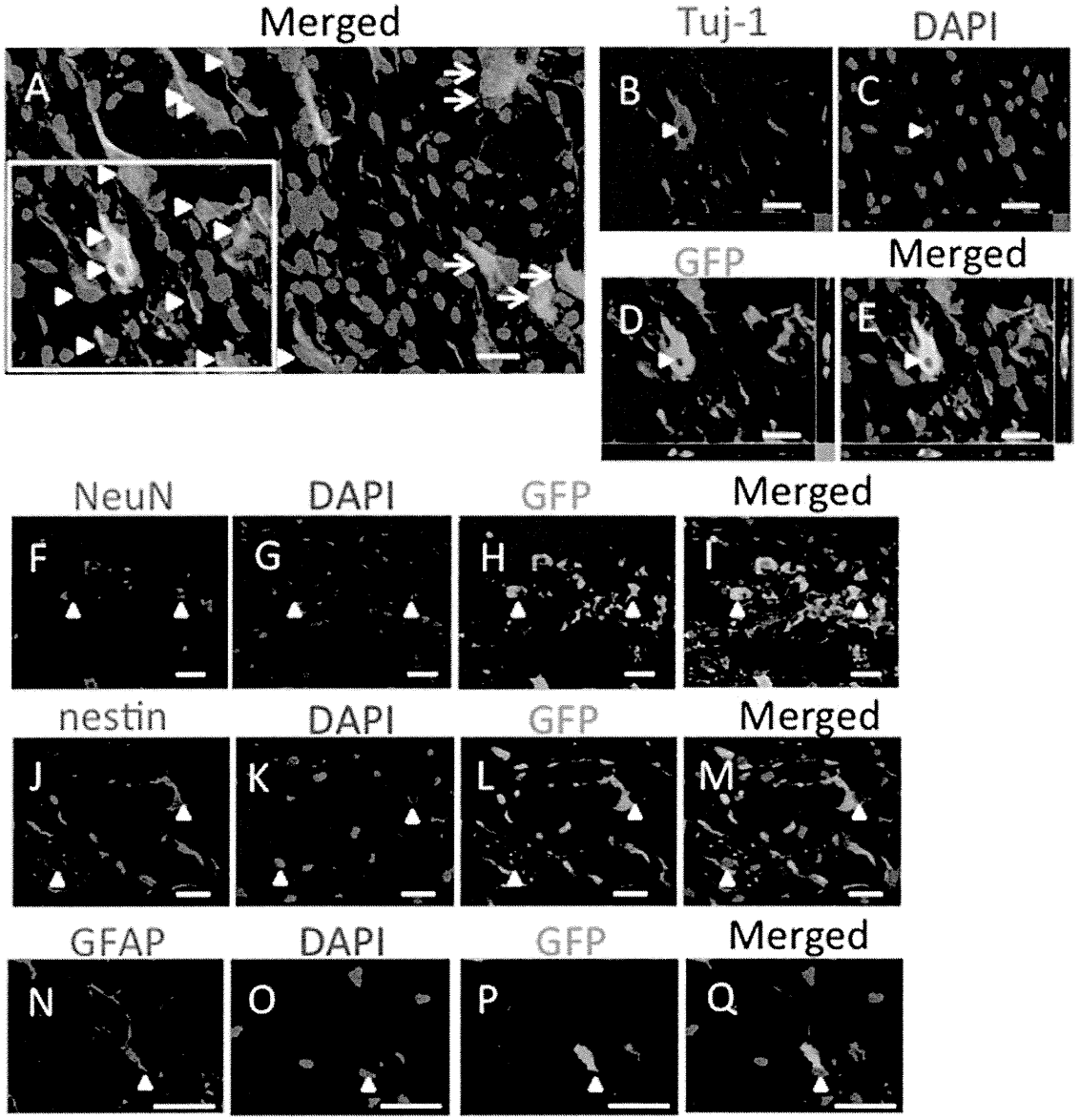

Figure 4. Differentiation of green fluorescent protein (GFP)-positive bone marrow-derived neural progenitor cells (BM-NPCs) in the spinal cord 8 weeks after injury. (A–Q) Cells labeled with neuron-specific class III β-tubulin (antibody: Tuj-1) (A–E) and neuronal nuclei (NeuN) (F–I) were encountered more frequently than those labeled with nestin (J–M) or glial fibrillary acidic protein (GFAP) (N–Q). Arrowheads, positively labeled cells. Arrows, GFP-positive and Tuj-1-negative cells. DAPI, 4′,6-diamidino-2-phenylindole. Scale bars: 20 μm.

Functional MRI Was Not Able to Provide Evidence of Reconstruction of Local Neuronal Networks After BM-NPC Transplantation

In response to electrical stimulation to the hind limbs, we counted fMRI signals in the bilateral somatosensory cortex in both BM-NPC and vehicle groups. BOLD signal changes were as high as 2.4% in the original hind limb territory in the BM-NPC group (Fig. 9). In the contralateral hind limb territory (HL) as defined in Figure 9B (36), volumes of activation in the BM-NPC group were significantly larger than those in the vehicle group ($p=0.014$, Student's t test) (Fig. 9C). Particularly, we noticed that cortical activation in spinally injured rats was not confined to the original hind limb territory in the primary somatosensory cortex (Fig. 9D). Signals extended more medially and even to the ipsilateral side of stimulation. Total volumes of cortical activation were 1.53 ± 0.83 and 0.41 ± 0.17 mm^3 in the BM-NPC and vehicle groups, respectively, while the difference was not statistically significant ($p=0.11$, Student's t test).

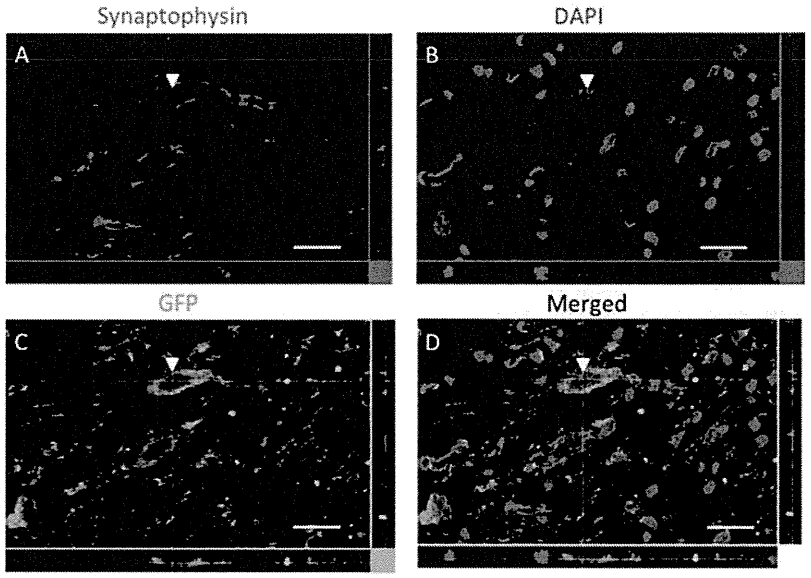

Figure 5. Synaptophysin expressed around GFP-positive bone marrow-derived neural progenitor cells (BM-NPCs). Photomicrographs depicting synaptophysin (A), DAPI (B), GFP (C), and a merged image (D) staining of transplanted cells in the spinal cord. This finding suggests the synapse formation between the transplanted cells and host cells. Arrowheads indicate positively labeled cells. Abbreviations are as in Figure 4. Scale bars: 20 μm.

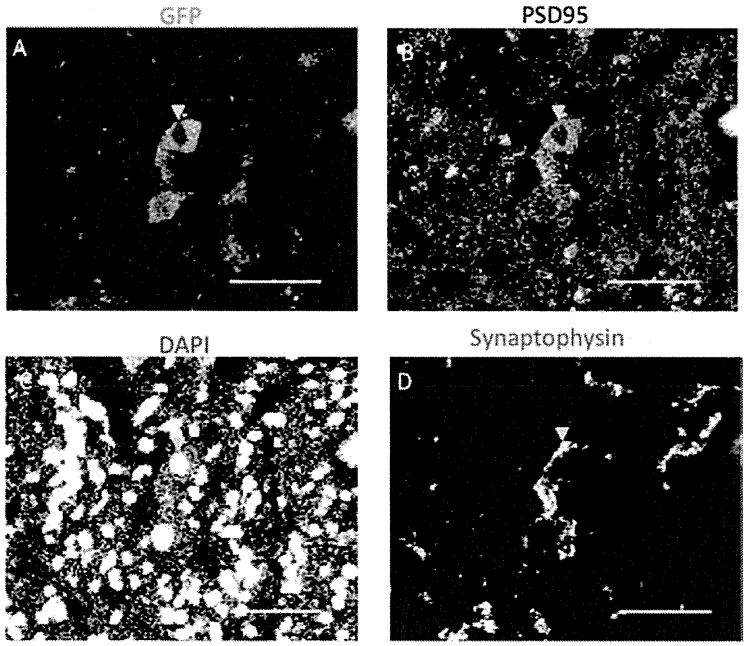

Figure 6. Postsynaptic density (PSD-95) localized adjacent to synaptophysin on GFP-positive bone marrow-derived neural progenitor cells (BM-NPCs). Photomicrographs depicting GFP (A), PSD-95 (B), DAPI (C), and synatophysin (D) staining of cells in the spinal cord. This finding suggests synapse formation between the transplanted cells and host cells. Arrowheads indicate positively labeled cells. Abbreviations are as in Figure 4. Scale bars: 50 μm.

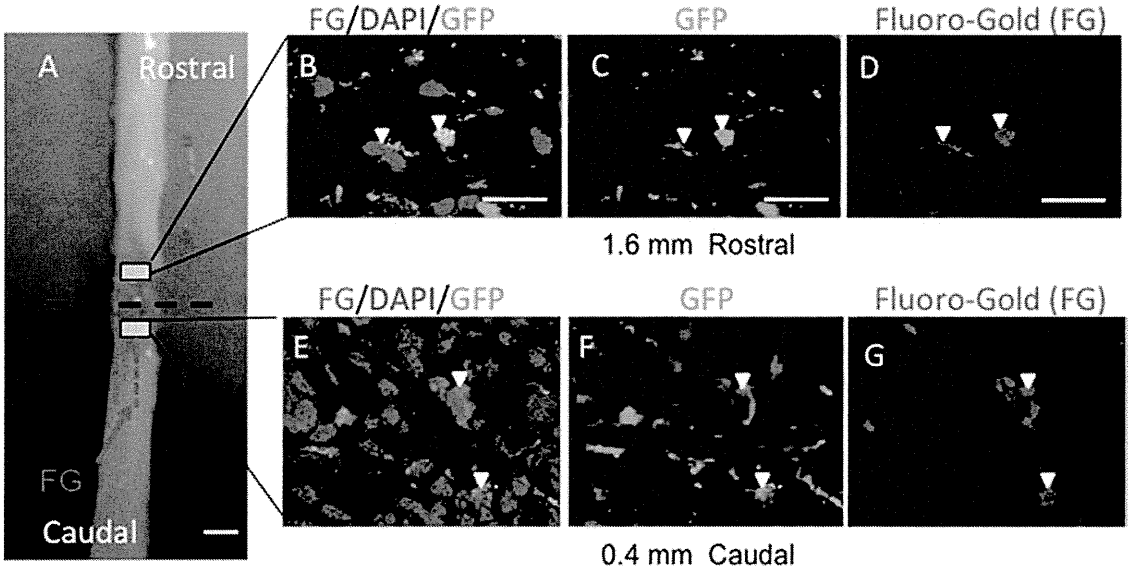

Figure 7. Expression of the retrograde tracer Fluorogold (FG) injected 10 mm caudal to the transected site of the spinal cord. (A) Schematic drawing of a representative spinal cord taken from the bone marrow-derived neural progenitor cell (BM-NPC) group, showing sites of FG injection (red arrow). Red dotted lines indicate the supposed routes by which FG was transported from the terminals of extended neurites and crossed the transected portion. (B–G) Green fluorescent protein (GFP)-positive BM-NPCs, transplanted rostral (B–D) and caudal (E–G) to the injured site, were also positive for FG in representative sections obtained 1.6 mm rostral and 0.4 mm caudal to the transected site. Abbreviations, schematic drawings, and arrowheads are as described in Figures 2 and 3. Scale bars: 2.0 mm (A) and 20 μm (B–G).

DISCUSSION

In this study, we report that transplantation of BM-NPCs promoted functional recovery of the spinally injured animals evidenced by improved locomotor scores. The grafted cells survived and committed predominant neuronal differentiation in the injured spinal cord. Immunohistochemistry using synaptophysin and PSD-95 as well as the FG tracing indicated synaptic formation of the BM-NPCs with the surrounding neurons and extension of the neurites across the transected portion in the spinal cord. As a consequence, neuronal networks were partially restored 7 weeks posttransplantation, which was represented as increased cortical signals in fMRI of the BM-NPC transplanted animals. However, the representation of the cortical signals was diverse and altered when compared to the original sensory map. Therefore, reestablishment of neuronal networks by transplantation of BM-NPCs was not fully accomplished.

Here, we demonstrated that transplantation of BM-NPCs was an efficient method in supplying neuronal lineage cells in a severely injured spinal cord. Majority of sphere-derived cells cultured with several trophic factors were reported to express neuronal markers such as βIII tubulin (Tuj-1) and microtubule associated protein 2 in a high ratio

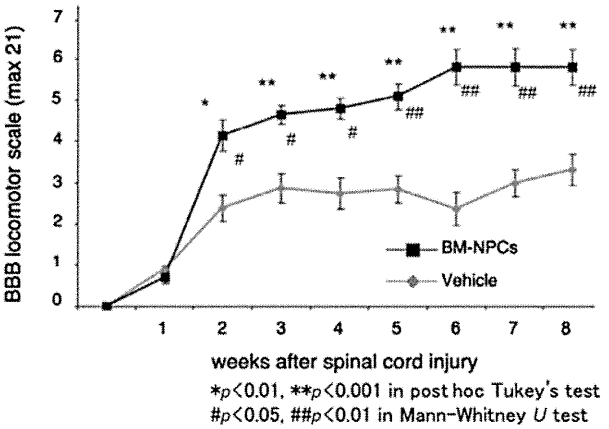

Figure 8. Basso, Beattie, Bresnahan (BBB) locomotor scale. Open-field locomotor hind limb function of all rats was tested on the day after injury and then weekly for 8 weeks postoperatively. Results are shown separately for groups transplanted on day 9 with bone marrow-derived neural progenitor cells (BM-NPCs) ($n=10$) or injected with vehicle ($n=14$). Repeated measures ANOVA followed by the post hoc Tukey's test as well as Mann–Whitney U test showed significant differences between the groups. Two weeks after injury, BBB scores of the BM-NPC group were significantly higher than those of the vehicle group. $*p<0.01$, $**p<0.001$ post hoc Tukey's test. $\#p<0.05$, $\#\#p<0.01$ Mann–Whitney U test.

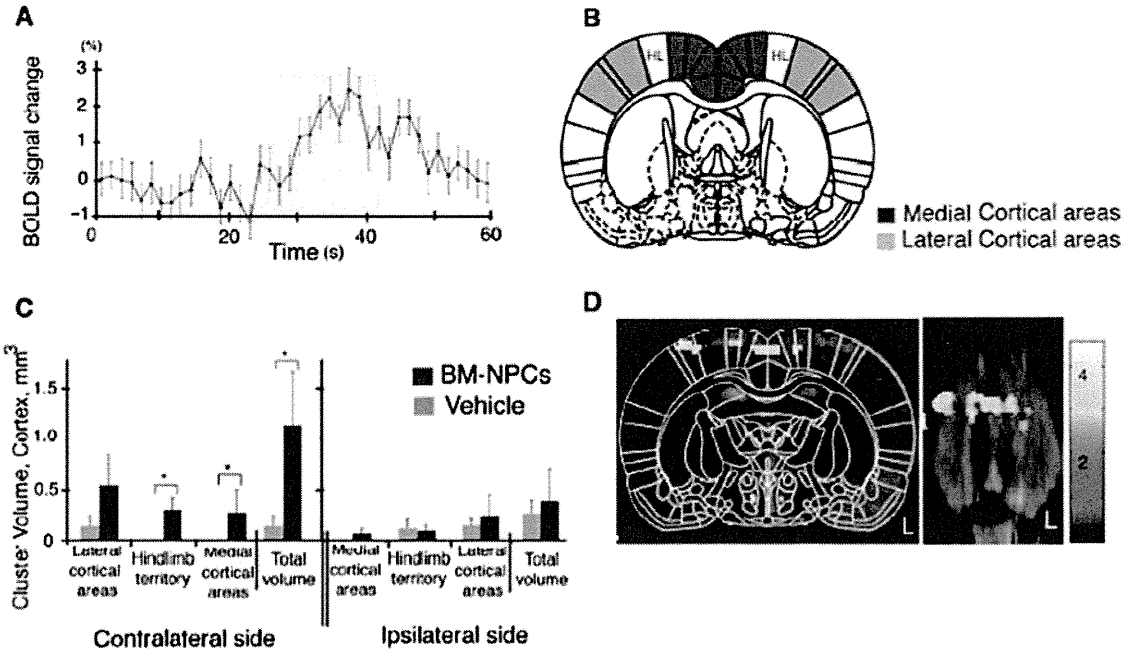

Figure 9. Cortical fMRI signals in response to hind limb stimulation 8 weeks after spinal cord transection. (A) Time course of blood oxygenation level-dependent (BOLD) signals (%) in a voxel in the original hind limb territory in the bone marrow-derived neural progenitor cell (BM-NPC) transplantation group ($n=6$). Gray bars indicate the period of stimulation. (B) Schematic drawing of a rat brain to illustrate medial cortical areas (dark gray), the hind limb territory of the primary somatosensory cortex area (HL) and lateral cortical areas (light gray), in which cortical activations were counted. (C) Volumes of functional magnetic resonance imaging (fMRI) signals in vehicle and BM-NPC groups. Significant differences between the BM-NPC and vehicle injection groups were noted in the signals in the contralateral cortex and the hind limb territory of the contralateral side to the stimulation ($*p<0.05$). Note that broad cortical areas were activated in response to hind limb stimulation 8 weeks after spinal cord injury. (D) A representative cortical sensory map from the BM-NPCs group, demonstrating neuronal activation in various cortical areas outside of the original hind limb territory in the primary somatosensory cortex. Signals were observed on the left side (L), which was ipsilateral to the stimulation as demonstrated in a coronal section (left) at bregma −1.4 mm and a horizontal section (right). The color scale indicates T statistics calculated by statistical parametric mapping software (SPM2). The coronal sections are superimposed on a schematic brain section from the same level [reproduced with permission of Elsevier from the Paxinos and Watson atlas (36)].

(98.5% and 95.7%, respectively) and GFAP in a low ratio (0.7%) (17). These findings clearly indicated that cells in the BM-NPC-derived spheres tended to differentiate into neurons and were not initially committed to the glial fate. In the same study in which BM-NPC-derived spheres were transplanted into the rat stroke model, BM-NPCs predominantly differentiated into NeuN-expressing postmitotic neurons (79.5%), and only a small population of the transplanted cells expressed GFAP (1.9%) (17). In the present study, we found that the rate of the differentiation of the transplanted GFP-positive cells into the neuronal fate detected by Tuj-1-positive cells was 77.2%; however, that of postmitotic neurons positive for NeuN was only 36.0%. The rate of differentiation into GFAP-positive astrocytes was 2.9%, similar to that observed in the transplantation into the rat stroke model. These observations indicate that, although the ratio of the differentiation into postmitotic neurons was dependent on the disease models, the BM-NPC-derived sphere cells predominantly differentiate into the neuronal fate after transplantation.

In general, the environment of the spinal cord is not permissive for survival and neuronal differentiation of the transplanted cells (19,27). Exogenous neural stem cells undergo proliferation and differentiate mainly into astrocytes in the spinal cord (33). When naive neural stem cells were transplanted into the injured spinal cord, 84% of the cells were GFAP-positive 9 weeks after transplantation, while only 4% of the cells had neuronal characteristics (18). Even when cells are shown to differentiate into neuronal lineage cells in vitro, the degree of neural induction in vivo may turn out to be less than expected after transplantation into the injured spinal cord (7). Our findings indicate that BM-NPCs are a reliable source of neuronal cells that can be used in cell transplantation therapy for SCI. Previously, we transplanted BM-NPCs and naive BMSCs in a rat stroke model and compared the results (17), in which BM-NPCs demonstrated much higher efficacy in survival, differentiation, and integration into the host brain. Having established the difference between BM-NPCs and naive BMSCs, we solely used BM-NPCs in the current protocol.

As Abematsu et al. demonstrated recently, grafted neuronal cells may establish neuronal connectivity by making synaptic connections with endogenous surrounding neurons (1). In this study, immunohistochemistry for synaptophysin and PSD-95 revealed the adjacent localization of synaptophysin and PSD-95 in the same GFP-positive transplanted cells (Fig. 6). Synaptophysin and PSD-95 are markers for presynaptic vesicles and postsynaptic density, respectively, suggesting that the transplanted cells constructed synaptic connections and received synaptic inputs from host and/or surrounding neurons.

In our model, retrograde axonal tracing showed the presence of cells double positive for FG and GFP in the spinal cord rostral to the transected portion. However, no FG-positive cells were detected in cervical spinal cord or brain sections, when we performed histological analyses 4 days following the injection of FG. In a previous report using a matrix seeded with BMSCs to fill the gap of the spinal cord transection injury, FG-labeled neurons were detected in the cortex and in the brainstem a week after the FG injection (22). With regard to the time between the FG injections and histological analyses, 4 days might not be long enough for the retrograde tracers to reach the brain stem through the severely injured spinal cord. Therefore, the purpose of the FG tracing was focused on evaluating grafted BM-NPCs located rostral to the transected stump. To avoid confusion in interpreting results, we only injected FG caudally and 10 mm from the stump. In this way, we could minimize the possibility that the tracer would diffuse and go across the transected portion (22). Results of the FG thus indicated that the grafted cells survived, differentiated, and might have extended neurites across the transected portion of the spinal cord.

Furthermore, the FG-labeled BM-NPCs localized 4.6 mm rostral to the spinal cord stump. Recently, we demonstrated the capacity of migration of BM-NPCs in a rat model of stroke (17). In spinal cord, various studies using in vivo MRI tracking systems have observed that the transplanted cells could actually migrate long distances. In one of these study, injected live cells traveled as far as 9 mm in 8 weeks following the transplantation (23). Although it is possible that dispersion might have transferred the grafted cells a few millimeters, the aforementioned information suggested that the BM-NPCs had the capacity to migrate in the spinal cord.

In this study, transplantation of BM-NPCs to the completely transected adult rat spinal cord led to a significant, albeit modest improvement of hind limb motor function as determined by BBB scoring. Eight weeks after the injury, the BBB score of injured animals was 3.3 without BM-NPC transplantation, while with the transplantation, it improved to 5.8. In other studies, BMSC-derived Schwann cells or olfactory mucosa were transplanted into similar complete spinal cord transection models in Wistar rats. In those studies, BBB scores were 3.6 and 2.6 in the controls, while 7.0 and 4.6 in the treatment groups, respectively (3,20). Degrees of improvement in BBB scores by BM-NPC transplantations were therefore comparable to those of the other studies. Importantly, to judge degrees of locomotor recovery by the BBB scores needs caution, since functional improvement may also depend on the strains used or the types of treatments applied. For instance, in Sprague–Dawley strains, BBB scores were lower and between 0 and 2 following complete transection of the spinal cord (13,26,41). In one of these studies, 10 weeks posttransplantation of olfactory ensheathing cells, BBB scores improved to 4.3 from 1.0 (26).

FMRI also demonstrated an increase of BOLD signals in cortex cerebri in response to electrical stimulation of a hind limb. In particular, cortical activations were not only observed in the original somatosensory cortex, rather the BOLD signals had an abnormal and diverse distribution, including ipsilateral activity. Together, the addition of the BM-NPCs to the injury area might lead to the reestablishment of a degree of ascending and descending neurotransmission across injury, while we could not confirm reconstruction of the disrupted neuronal networks by the distribution of recovered cortical activations in fMRI.

One of the reasons for such ambiguity could partly rely on the end point of this study, which was 7 weeks posttransplantation. In the current methods, we set the end point mainly based on the time course of locomotor recovery. As shown in Figure 8, BBB scores improved and reached a plateau 5–6 weeks after the transplantation. In another experiment using fMRI to evaluate sensory recovery in a rat model of SCI, fMRI was performed 9 weeks posttransplantation, which demonstrated recovery of cortical responses (18). Moreover, in our previous experiment applying BMSC-derived Schwann cells to a rat model of complete spinal cord transection, it was 6 weeks posttransplantation when the axonal regeneration was histologically confirmed (20). However, as we demonstrated previously, reorganization in cerebral cortex may take place over 6 months long after SCI (13). After severe thoracic SCI, cortical connections from the spared forelimbs expanded and took over the deafferented hind limb areas (13,16). If such deafferentation plasticity occurs, the corresponding somatosensory cortex may no longer be available to receive or process recovered ascending sensory information. In this sense, the time allowed for recovery following the complete transection could be too short and limit the value of fMRI in this study.

Another possible explanation for the diverse cortical signals in fMRI is misdirection of sensory inputs through the reconstructed neuronal networks. After transplantation of BM-NPCs, new synaptic pathways relaying peripheral inputs to cortical areas were formed in the injured spinal cord. However, they could be different from those in the original ascending tracts. In such a situation, recovered

sensory inputs would not connect with the original hind limb territory, but with various cortical areas.

Besides specific neuronal cell induction, another possible strategy for treating SCI includes transduction of neural stem cells into the oligodendrocytic lineage to enhance myelination (18,21). Using this approach, myelination of spared axons led to recovery of conduction velocity and promoted functional recovery in SCI. Hypothetically, however, if axons are completely severed in the damaged spinal cord, as occurs in our injury model and a model used by others (1), enhancement of myelination with oligodendrocytes may have limited effectiveness. In this situation, a strategy in which added neuronal cells may serve as a form of interneuron providing a link across the injury may be a more reliable approach. Depending on the degree of injury, one may need to select or combine different types of cell transplantation to achieve the best functional recovery.

We conclude that delayed grafting of BM-NPCs into the injured spinal cord was effective in providing neuronal lineage cells. If an efficient neuronal induction in the injured spinal cord was feasible, reconstruction of disrupted neuronal circuits between grafted cells and endogenous surrounding neurons can be a possible means of achieving recovery from SCI. Depending on the degrees of SCI, we can select or combine different types of cell transplantation to achieve the best functional recovery in SCI and other neural degenerative diseases occurring in the spinal cord.

ACKNOWLEDGMENTS: We thank Ms. Ryoko Mamiya for her technical assistance and Dr. Mitsunobu Matsubara and Dr. Kuniyasu Niizuma (Tohoku University) for their useful inputs to our project. This work was supported by Program for Promotion of Fundamental Studies in Health Sciences of the National Institute of Biomedical Innovation (NIBIO). This work was supported by Program for Promotion of Fundamental Studies in Health Sciences of the National Institute of Biomedical Innovation (NIBIO). The authors declare no conflict of interest.

REFERENCES

1. Abematsu, M.; Tsujimura, K.; Yamano, M.; Saito, M.; Kohno, K.; Kohyama, J.; Namihira, M.; Komiya, S.; Nakashima, K. Neurons derived from transplanted neural stem cells restore disrupted neuronal circuitry in a mouse model of spinal cord injury. J. Clin. Invest. 120:3255–3266; 2010.
2. Ankeny, D. P.; McTigue, D. M.; Jakeman, L. B. Bone marrow transplants provide tisssue protection and directional guidance for axons after contusive spinal cord injury in rats. Exp. Neurol. 190:17–31; 2004.
3. Aoki, M.; Kishima, H.; Yoshimura, K.; Ishihara, M.; Ueno, M.; Hata, K.; Yamashita, T.; Iwatsuki, K.; Yoshimine, T. Limited functional recovery in rats with complete spinal cord injury after transplantation of whole-layer olfactory mucosa: Laboratory investigation. J. Neurosurg. Spine 12: 122–130; 2010.
4. Azizi, S. A.; Stokes, D.; Augelli, B. J.; DiGirolamo, C.; Prockop, D. J. Engraftment and migration of human bone marrow stromal cells implanted in the brains of albino rats—similarities to astrocyte grafts. Proc. Natl. Acad. Sci. USA 95(7):3908–3913; 1998.
5. Baptiste, D. C.; Fehlings, M. G. Update on the treatment of spinal cord injury. Prog. Brain Res. 161:217–233; 2007.
6. Basso, D. M.; Beattie, M. S.; Bresnahan, J. C. A sensitive and reliable locomotor rating scale for open field testing in rats. J. Neurotrauma 12:1–21; 1995.
7. Cao, Q. L.; Howard, R. M.; Dennison, J. B.; Whittemore, S. R. Differentiation of engrafted neuronal-restricted precursor cells is inhibited in the traumatically injured spinal cord. Exp. Neurol. 177:349–359; 2002.
8. Cheng, C.; Gao, S.; Zhao, J.; Niu, S.; Chen, M.; Li, X.; Qin, J.; Shi, S.; Guo, Z.; Shen, A. Spatiotemporal patterns of postsynaptic density (PSD)-95 expression after rat spinal cord injury. Neuropathol. Appl. Neurobiol. 34:340–356; 2007.
9. Dezawa, M.; Hoshino, M.; Nabeshima, Y.; Ide, C. Marrow stromal cells: Implications in health and disease in the nervous system. Curr. Mol. Med. 5:723–732; 2005.
10. Dezawa, M.; Kanno, H.; Hoshino, M.; Cho, H.; Matsumoto, N.; Itokazu, Y.; Tajima, N.; Yamada, H.; Sawada, H.; Ishikawa, H.; Mimura, T.; Kitada, M.; Suzuki, Y.; Ide, C. Specific induction of neuronal cells from bone marrow stromal cells and application for autologous transplantation. J. Clin. Invest. 113:1701–1710; 2004.
11. Ding, D. C.; Shyu, W. C.; Lin, S. Z. Mesenchymal stem cells. Cell Transplant. 20:5–14; 2011.
12. Endo, T.; Spenger, C.; Hao, J.; Tominaga, T.; Wiesenfeld-Hallin, Z.; Olson, L.; Xu, X. J. Functional MRI of the brain detects neuropathic pain in experimental spinal cord injury. Pain 138:292–300; 2008.
13. Endo, T.; Spenger, C.; Tominaga, T.; Brene, S.; Olson, L. Cortical sensory map rearrangement after spinal cord injury: fMRI responses linked to Nogo signalling. Brain 130:2951–2961; 2007.
14. Filbin, M. T. Myelin-associated inhibitors of axonal regeneration in the adult mammalian CNS. Nat. Rev. Neurosci. 4:703–713; 2003.
15. Fitch, M. T.; Silver, J. CNS injury, glial scars, and inflammation: Inhibitory extracellular matrices and regeneration failure. Exp. Neurol. 209:294–301; 2008.
16. Ghosh, A.; Haiss, F.; Sydekum, E.; Schneider, R.; Gullo, M.; Wyss, M. T.; Mueggler, T.; Baltes, C.; Rudin, M.; Weber, B.; Schwab, M. E. Rewiring of hindlimb corticospinal neurons after spinal cord injury. Nat. Neurosci. 13:97–104; 2010.
17. Hayase, M.; Kitada, M.; Wakao, S.; Itokazu, Y.; Nozaki, K.; Hashimoto, N.; Takagi, Y.; Dezawa, M. Committed neural progenitor cells derived from genetically modified bone marrow stromal cells ameliorate deficits in a rat model of stroke. J. Cereb. Blood Flow Metab. 29:1409–1420; 2009.
18. Hofstetter, C. P.; Holmstrom, N. A.; Lilja, J. A.; Schweinhardt, P.; Hao, J.; Spenger, C.; Wiesenfeld-Hallin, Z.; Kurpad, S. N.; Frisen, J.; Olson, L. Allodynia limits the usefulness of intraspinal neural stem cell grafts; directed differentiation improves outcome. Nat. Neurosci. 8:346–353; 2005.
19. Johnson, P. J.; Tatara, A.; Shiu, A.; Sakiyama-Elbert, S. E. Controlled release of neurotrophin-3 and platelet-derived growth factor from fibrin scaffolds containing neural progenitor cells enhances survival and differentiation into neurons in a subacute model of SCI. Cell Transplant. 19: 89–101; 2010.
20. Kamada, T.; Koda, M.; Dezawa, M.; Yoshinaga, K.; Hashimoto, M.; Koshizuka, S.; Nishio, Y.; Moriya, H.; Yamazaki, M. Transplantation of bone marrow stromal cell-derived Schwann cells promotes axonal regeneration and functional recovery after complete transection of adult rat spinal cord. J. Neuropathol. Exp. Neurol. 64:37–45; 2005.

21. Keirstead, H. S.; Nistor, G.; Bernal, G.; Totoiu, M.; Cloutier, F.; Sharp, K.; Steward, O. Human embryonic stem cell-derived oligodendrocyte progenitor cell transplants remyelinate and restore locomotion after spinal cord injury. J. Neurosci. 25:4694–4705; 2005.
22. Kosacka, J.; Nowicki, M.; Kacza, J.; Borlak, J.; Engele, J.; Borowski, K. S. Adipocyte-derived angiopoietin-1 supports neurite outgrowth and synaptogenesis of sensory neurons. J. Neurosci. Res. 83:1160–1169; 2006.
23. Lee, I. H.; Bulte, J. W.; Schweinhardt, P.; Douglas, T.; Trifunovski, A.; Hofstetter, C.; Olson, L.; Spenger, C. In vivo magnetic resonance tracking of olfactory ensheathing glia grafted into the rat spinal cord. Exp. Neurol. 187:509–516; 2004.
24. Liang, H.; Liang, P.; Xu, Y.; Wu, J.; Liang, T.; Xu, X. DHAM-BMSC matrix promotes axonal regeneration and functional recovery after spinal cord injury in adult rats. J. Neurotrauma 26:1745–1757; 2009.
25. Lilja, J.; Endo, T.; Hofstetter, C.; Westman, E.; Young, J.; Olson, L.; Spenger, C. Blood oxygenation level-dependent visualization of synaptic relay stations of sensory pathways along the neuroaxis in response to graded sensory stimulation of a limb. J. Neurosci. 26:6330–6336; 2006.
26. Lu, J.; Feron, F.; Mackay-Sim, A.; Waite, P. M. Olfactory ensheathing cells promote locomotor recovery after delayed transplantation into transected spinal cord. Brain 125:14–21; 2002.
27. Ma, Y. H.; Zhang, Y.; Cao, L.; Su, J. C.; Wang, Z. W.; Xu, A. B.; Zhang, S. C. Effect of neurotrophin-3 genetically modified olfactory ensheathing cells transplantation on spinal cord injury. Cell Transplant. 19:167–177; 2010.
28. Matsuse, D.; Kitada, M.; Ogura, F.; Wakao, S.; Kohama, M.; Kira, J.; Tabata, Y.; Dezawa, M. Combined transplantation of bone marrow stromal cell-derived neural progenitor cells with a collagen sponge and basic fibroblast growth factor releasing microspheres enhances recovery after cerebral ischemia in rats. Tissue Eng. Part A 17:1993–2004; 2011.
29. Nguyen, T. H.; Khakhoulina, T.; Simmons, A.; Morel, P.; Trono, D. A simple and highly effective method for the stable transduction of uncultured porcine hepatocytes using lentiviral vector. Cell Transplant. 14:489–496; 2005.
30. Ogawa, S.; Menon, R. S.; Tank, D. W.; Kim, S. G.; Merkle, H.; Ellermann, J. M.; Ugurbil, K. Functional brain mapping by blood oxygenation level-dependent contrast magnetic resonance imaging. A comparison of signal characteristics with a biophysical model. Biophys. J. 64:803–812; 1993.
31. Okano, H.; Ogawa, Y.; Nakamura, M.; Kaneko, S.; Iwanami, A.; Toyama, Y. Transplantation of neural stem cells into the spinal cord after injury. Semin. Cell. Dev. Biol. 14:191–198; 2003.
32. Olson, L. Regeneration in the adult central nervous system: Experimental repair strategies. Nat. Med. 3:1329–1335; 1997.
33. Parr, A. M.; Kulbatski, I.; Tator, C. H. Transplantation of adult rat spinal cord stem/progenitor cells for spinal cord injury. J. Neurotrauma 24:835–845; 2007.
34. Parr, A. M.; Tator, C. H.; Keating, A. Bone marrow-derived mesenchymal stromal cells for the repair of central nervous system injury. Bone Marrow Transplant. 40:609–619; 2007.
35. Pawela, C. P.; Biswal, B. B.; Hudetz, A. G.; Li, R.; Jones, S. R.; Cho, Y. R.; Matloub, H. S.; Hyde, J. S. Interhemispheric neuroplasticity following limb deafferentation detected by resting-state functional connectivity magnetic resonance imaging (fcMRI) and functional magnetic resonance imaging (fMRI). Neuroimage 49:2467–2478; 2010.
36. Paxinos, G.; Watson, C. The rat brain in stereotaxic coordinates, the new coronal set, fifth ed. New York: Academic Press; 2005.
37. Sanganahalli, B. G.; Bailey, C. J.; Herman, P.; Hyder, F. Tactile and non-tactile sensory paradigms for fMRI and neurophysiologic studies in rodents. Methods. Mol. Biol. 489:213–242; 2009.
38. Schweinhardt, P.; Fransson, P.; Olson, L.; Spenger, C.; Andersson, J. L. A template for spatial normalisation of MR images of the rat brain. J. Neurosci. Methods 129:105–113; 2003.
39. Shimizu, S.; Kitada, M.; Ishikawa, H.; Itokazu, Y.; Wakao, S.; Dezawa, M. Peripheral nerve regeneration by the in vitro differentiated-human bone marrow stromal cells with Schwann cell property. Biochem. Biophys. Res. Commun. 359:915–920; 2007.
40. Spenger, C.; Josephson, A.; Klason, T.; Hoehn, M.; Schwindt, W.; Ingvar, M.; Olson, L. Functional MRI at 4.7 tesla of the rat brain during electric stimulation of forepaw, hindpaw, or tail in single- and multislice experiments. Exp. Neurol. 166:246–253; 2000.
41. Steward, O.; Sharp, K.; Selvan, G.; Hadden, A.; Hofstadter, M.; Au, E.; Roskams, J. A reassessment of the consequences of delayed transplantation of olfactory lamina propria following complete spinal cord transection in rats. Exp. Neurol. 198:483–499; 2006.
42. Sumiyoshi, A.; Riera, J. J.; Ogawa, T.; Kawashima, R. A mini-cap for simultaneous EEG and fMRI recording in rodents. Neuroimage 54:1951–1965; 2011.
43. von Bohlen Und Halbach, O. Immunohistological markers for staging neurogenesis in adult hippocampus. Cell Tissue Res. 329:409–420; 2007.
44. Wang, G.; Ao, Q.; Gong, K.; Zuo, H.; Gong, Y.; Zhang, X. Synergistic effect of neural stem cells and olfactory ensheathing cells on repair of adult rat spinal cord injury. Cell Transplant. 19:1325–1337; 2010.
45. Yiu, G.; He, Z. Glial inhibition of CNS axon regeneration. Nat. Rev. Neurosci. 7:617–627; 2006.

Isolation, culture and evaluation of multilineage-differentiating stress-enduring (Muse) cells

Yasumasa Kuroda[1,3], Shohei Wakao[2,3], Masaaki Kitada[2,3], Toru Murakami[2], Makoto Nojima[2] & Mari Dezawa[1,2]

[1]Department of Anatomy and Anthropology, Tohoku University Graduate School of Medicine, Sendai, Japan. [2]Department of Stem Cell Biology and Histology, Tohoku University Graduate School of Medicine, Sendai, Japan. [3]These authors contributed equally to this work. Correspondence should be addressed to Y.K. (y-kuroda@med.tohoku.ac.jp), M.K. (masaaki.kitada@gmail.com) or M.D. (mdezawa@med.tohoku.ac.jp).

Published online 20 June 2013; doi:10.1038/nprot.2013.076

Multilineage-differentiating stress-enduring (Muse) cells are distinct stem cells in mesenchymal cell populations with the capacity to self-renew, to differentiate into cells representative of all three germ layers from a single cell, and to repair damaged tissues by spontaneous differentiation into tissue-specific cells without forming teratomas. We describe step-by-step procedures for isolating and evaluating these cells. Muse cells are also a practical cell source for human induced pluripotent stem (iPS) cells with markedly high generation efficiency. They can be collected as cells that are double positive for stage-specific embryonic antigen-3 (SSEA-3) and CD105 from commercially available mesenchymal cells, such as adult human bone marrow stromal cells and dermal fibroblasts, or from fresh adult human bone marrow samples. Under both spontaneous and induced differentiation conditions, they show triploblastic differentiation. It takes 4–6 h to collect and 2 weeks to confirm the differentiation and self-renewal capacity of Muse cells.

INTRODUCTION

Mesenchymal stem cells (MSCs) are tissue stem cells that reside in mesenchymal tissues and that have attracted attention because of their unique properties. Generally, tissue stem cells are known to differentiate into the cell types of the tissue in which they reside; neural stem cells differentiate into neurons and glial cells, and hematopoietic stem cells give rise to all blood cell types[1,2]. Distinct from these tissue stem cells, MSCs have been reported to have the broad-ranged differentiation ability that crosses the oligolineage boundaries between the mesodermal and ectodermal or endodermal lineages[3,4]. In particular, the differentiation ability of bone marrow stromal cells (BMSCs), which are cultured as adherent cells from bone marrow aspirates, has been studied from the late 1990s up to the present time. BMSCs *in vitro* have been reported to give rise to cells not only in the same mesodermal lineage (osteocytes, chondrocytes, adipocytes[5,6], skeletal muscle cells[7–9], cardiac muscle cells[10,11] and endothelial cells[12,13]) but also in ectodermal (neuronal cells[14,15], Schwann cells[16,17]) and endodermal (hepatocytes[18,19], insulin-producing pancreatic beta cells[20,21]) lineages. In addition, when they are grafted into animals with tissue damage, BMSCs have been shown to spontaneously differentiate into and function as tissue-specific cells that replenish lost cells *in vivo*; therefore, BMSCs are presumed to act as the 'repairing cells'. This *in vivo* spontaneous differentiation has been demonstrated in skeletal muscle cells[22], cardiac muscle cells[23], neuronal cells[24], retinal cells[25], keratinocytes[26] and hepatocytes[27] after grafting, but as the efficiency of integration and differentiation is generally low, it is believed that only a particular subset of BMSCs can lead to such reparative effects. The similar differentiation abilities of mesenchymal cell populations have also been reported in adipose tissue[28], synovial tissue[29], dental pulp[30], umbilical cord[31] and dermis[32].

The above findings suggested that MSCs include a particular subset of stem cells that have the triploblastic differentiation ability that can give rise to various types of cells of all three germ layers and that can function as tissue-repairing cells *in vivo*. However, the 'stemness' of such cells has not been fully elucidated. The term 'MSCs' is generally used to represent cells that are collected from mesenchymal tissues by adherent culture, and therefore they are not composed of a single cell type but of crude heterogeneous cell populations. Classification as stem cells requires the presence of two fundamental properties: differentiation and self-renewal[33]. The triploblastic differentiation ability of MSCs mentioned above has largely been demonstrated by studies using crude heterogeneous MSCs, whose self-renewal property has not clearly been demonstrated[34,35]. Although there are some reports demonstrating the self-renewal property of a particular stem cell population of the MSCs, the differentiation ability presented in these studies was not triploblastic[36,37]. For these reasons, it has long been debated whether a specific stem cell population that shows both triploblastic differentiation and self-renewal capacity exists among MSCs[4,38].

Properties of Muse cells

Recently, we used a clonal analyis to identify a specific cell population that has a capacity for self-renewal and triploblastic differentiation similar to that of pluripotent stem cells in adult human mesenchymal cell populations[39]. We refer to this specific stem cell fraction as Muse cells because of their particular broad-ranged differentiation ability and stress tolerance. They can be collected as cells that are double-positive for the pluripotency marker SSEA-3 and the mesenchymal cell marker CD105 from commercially available mesenchymal cell populations, such as adult human BMSCs and dermal fibroblasts, or they can be collected from the mononuclear cell fraction of fresh adult human bone marrow aspirates. These cells express other pluripotency markers and have the property of self-renewal. A single Muse cell is able to give rise to not only mesodermal-lineage cells such as osteocytes, chondrocytes, adipocytes, smooth muscle cells and skeletal muscle cells but also ectodermal and endodermal cells such as neurons, epidermal cells, hepatocytes and biliary cells. Although these capacities of Muse cells are considered similar to those of other pluripotent stem cells, it is notable that, in contrast to embryonic stem (ES) cells or iPS cells, Muse cells are not immortal in culture or tumorigenic *in vivo*.

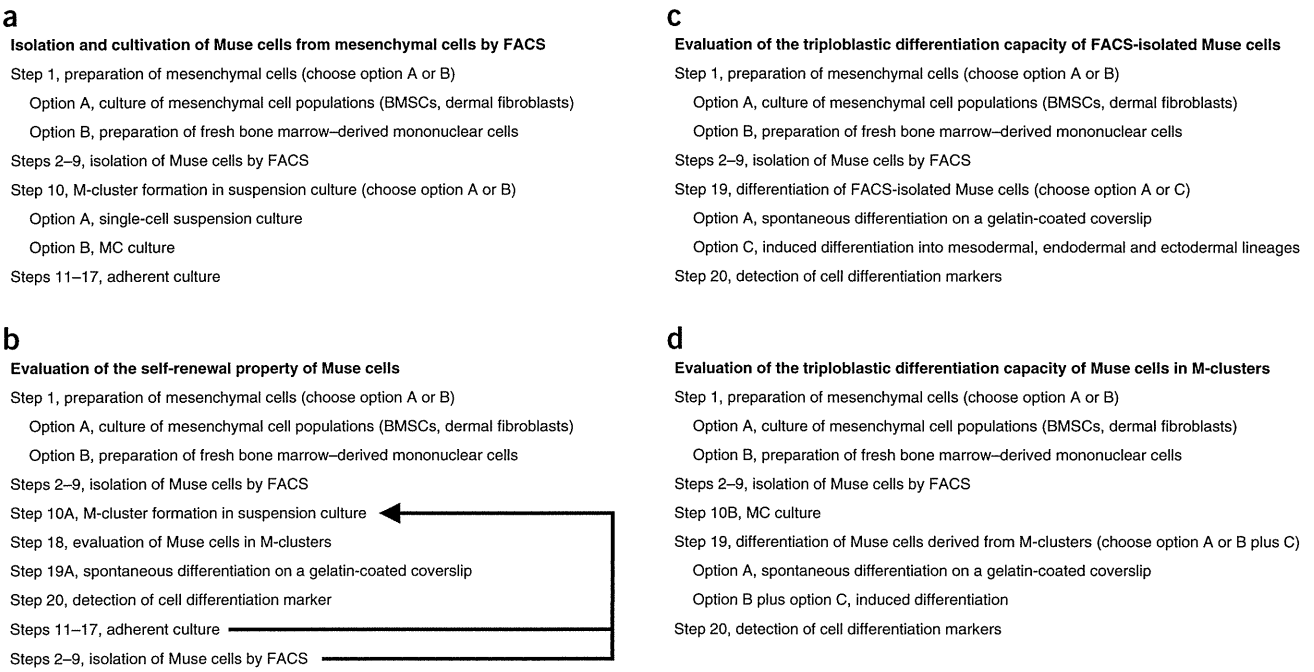

Figure 1 | Schematic overview of isolation, cultivation and evaluation of Muse cells.

Their telomerase activity is as low as that detected in adult dermal fibroblasts, and they do not form teratomas when transplanted into the testes of immunodeficient mice, as is often observed after transplantation of ES cells or iPS cells. *In vivo,* Muse cells can integrate into damaged tissues and spontaneously differentiate into tissue-specific marker–expressing cells according to the microenvironment when transplanted into animal models of fulminant hepatitis, skeletal muscle injury and skin injury[39]. Therefore, Muse cells are suggested to be the 'repairing cells' that have been postulated to exist among MSCs[39]. Another remarkable advantage of Muse cells is that they can be an efficient and practical cell source for iPS cell generation[40]. Adult human dermal fibroblast–derived Muse cells generated iPS cells with 30-fold higher efficiency than naive fibroblasts did, whereas cells other than Muse cells failed to form iPS cells, suggesting that Muse cells are virtually the original cell source for iPS cells among human dermal fibroblasts[40]. The unique capacities of Muse cells, including triploblastic differentiation, self-renewal, tissue repair without tumorigenic activity and high iPS cell–generation efficiency have great benefits not only in regenerative medicine but also in basic research into, for example, the full characterization of MSCs and the mechanisms of iPS cell generation.

Adult human mesenchymal tissues such as the bone marrow and dermis are known to contain several kinds of stem or progenitor cells such as multipotent adult progenitor cells, very small embryonic-like stem cells, marrow-isolated adult multilineage inducible cells, skin-derived precursors and CD146$^+$ osteoprogenitors[18,41–47], some of which are known to express pluripotency markers and are reported to have triploblastic differentiation ability similar to that of Muse cells[18,41–45]. However, the triploblastic differentiation ability of these stem cells has not been demonstrated at a single-cell level, as has been shown in Muse cells[40], so that pluripotentcy in the above-mentioned cell types has been, in the strict sense, an open question. The expression pattern of cell surface antigens in these stem cells is quite different from that in Muse cells, and, in particular, none of these stem cells express SSEA-3, by which Muse cells can be isolated directly from the adult mesenchymal tissue such as fresh bone marrow. Besides, when transplanted into the injured or degenerative tissues, Muse cells show high tissue-repairing activity, by which 80% or more Muse cells can differentiate into tissue-specific cell types, and they can replenish lost cells in damaged tissues[39]. A similarly high tissue-repairing activity has not been reported in the above-mentioned stem or progenitor cells. Thus, Muse cells are considered a distinct cell population from previously reported stem or progenitor cells among mesenchymal cell populations. Although some of the properties of Muse cells, namely self-renewal, triploblastic differentiation *in vitro* and tissue-repairing effect *in vivo,* have been clarified[39,40], future studies are required to elucidate the specific behavior of endogenous Muse cells, including the self-renewal property that has been demonstrated in a particular cell population of BMSCs[46,47], as well as their broad-ranged differentiation, the biological significance of the expression of pluripotency markers and the correlation between Muse cells and other tissue stem or progenitor cells.

Experimental design

We present here the protocol for isolation, cultivation and evaluation of Muse cells. A summary of our protocol is shown in **Figure 1**. We first describe the methods for preparation of mesenchymal cells (Step 1). In this section, the detailed protocol for culturing BMSCs and dermal fibroblasts is described (Step 1A), because the viability and isolation efficiency of Muse cells are highly dependent on the basic culture method of these mesenchymal cells. As Muse cells can be isolated from mononuclear cells from fresh bone marrow, the protocol for preparing